ELSEVIER

Coordination Chemistry Reviews
167 (1997) 1–48

COORDINATION CHEMISTRY REVIEWS

Thermodynamic and structural aspects of electrochemical deposition of metals and binary compounds in molten salts[1]

V. Danek *, M. Chrenková, A. Silný

Institute of Inorganic Chemistry, Slovak Academy of Sciences, Dúbravská cesta 9, 842 36 Bratislava, Slovak Republic

Received 18 December 1996; accepted 14 July 1997

Content

* *Corresponding author.*

[1] Based on the plenary lecture presented at the International Conference "Progress in Inorganic and Organometallic Chemistry", Polanica, Poland, September 19–23, 1994.

PII S0010-8545(97)00051-9

Abstract

The influence of the ionic structure of electrolytes used in the electrodeposition of molybdenum, titanium and aluminium on the mechanism and kinetics of metal deposition is discussed. Using electrochemical methods of study and a complex thermodynamic and physico-chemical analysis it was determined that in all the electrolytes investigated the electrodeposition process is significantly facilitated by the formation of complex anions with lower symmetry of the co-ordination sphere. In the case of molybdenum deposition, complex heteropolyanions are probably created in the melt by the addition of B_2O_3 or SiO_2 to the K_2MoO_4-based electrolytes. The electrodeposition of titanium from the K_2TiF_6-based electrolytes is enhanced by the formation of the less stable TiF_7^{3-}, resp. TiF_6Cl^{3-} anions. In the electrolysis of aluminium from cryolite–alumina melts the creation of oxyfluoroaluminate anions facilitates the electrodeposition of aluminium. © 1997 Elsevier Science S.A.

1. Introduction

The electrodeposition of metals from molten salts has been extensively studied for many decades. From an analysis of the literature it is clear that several types of molten systems have been tested as electrolytes. On the basis of the electroactive species used they can be divided into two principal groups:

(i) systems containing halo-complexes of the deposited metals,

(ii) systems containing oxides or oxy-complexes of the deposited metals.

In all of the systems investigated one of the most important tasks to be solved is to find the proper composition of the electrolyte with regard both to the suitable physico-chemical properties of the electrolyte and the desired characters of the electrodeposited product. Both problems are closely related to the actual structure, i.e. the ionic composition of the melt.

Quite recently attention was paid to the role of oxides, either as electroactive species, as impurities or as additives in the electrodeposition of metals. This may be demonstrated e.g. in the case of electrodeposition of molybdenum [1,2], where the electrolysis of neither pure K_2MoO_4, nor the $KF–K_2MoO_4$ mixture yields a molybdenum deposit. However, by introducing small amounts of boron oxide, or silicon dioxide to the basic melts, smooth and adherent molybdenum deposits may be obtained [2,3].

In the present review we study the influence of different additives which change the structure of the electrolyte (i.e. ionic composition) of the pure molten compound on the electrodeposition of molybdenum, titanium and aluminium using a voltammetric method. Based on measurements of the phase equilibrium, density, electrical conductivity and viscosity and using the complex physico-chemical analysis of the electrolytes, conclusions about the probable structure of electroactive species present in the electrolyte as well as on their electrochemical stability were made.

2. Thermodynamic approach

In general, the melts investigated represent multi-component systems of inorganic salts and oxides or oxygen-containing compounds, in which chemical reactions take

place. The chemical equilibrium in the melt depends on the composition and temperature. The influence of composition plays the most important role, while the change in temperature does not affect the equilibrium dramatically.

A physico-chemical analysis, based on the results of the measurements of phase equilibrium, density, electric conductivity and viscosity of the melts and combined with the electrochemical study of electrolytes, X-ray phase analysis and IR, resp. Raman spectroscopy of quenched melts, has been used for the study of the structure, i.e. the ionic composition of the molten systems under investigation. It may be assumed that the high temperature composition is at least qualitatively conserved after quenching.

To draw conclusions on the structure of the electrolytes from the concentration dependencies of the particular properties the following thermodynamical, statistical approaches and material balance calculation were used.

2.1. Dilute solutions

In the region of dilute solutions the limiting law is valid

$$\lim_{x \to 1} \frac{\partial a_i}{\partial x_i} = k(\mathrm{St}) \tag{1}$$

where a_i is the activity of the component expressed in terms of the mole fractions x_i's according to any suitable model and $k(\mathrm{St})$ is the correction factor introduced by Stortenbeker [4], representing the number of foreign particles, which introduces the solute into the solvent at infinite dilution. If $k(\mathrm{St}) = 1$, the investigated system obeys Raoult's law and belongs to the solution type No. I. If $k(\mathrm{St}) \neq 1$, the system belongs to type No. II, which do not obey Raoult's law.

The region of diluted solutions can be investigated preferentially by cryoscopic measurements. For the lowering of the temperature of fusion of the solvent, ΔT_f, the following equation holds

$$\Delta T_\mathrm{f} = \frac{RT_\mathrm{f}^2}{\Delta H_\mathrm{f}} x_\mathrm{B} \cdot k(\mathrm{St}) \tag{2}$$

where T_f and ΔH_f are the temperature and the enthalpy of fusion of the solvent, respectively, x_B is the mole fraction of the solvent, and R is the gas constant. The resulting knowledge of $k(\mathrm{St})$ enables one to deduce the possible ongoing chemical reaction between solvent and solute.

2.2. Whole systems

For the whole concentration region of the system investigated two different approaches may be used. In the first approach, the structure (i.e. the ionic composition) is determined by the thermodynamic equilibrium composition, after all the

chemical reactions taking place in the system are over. Ideal mixing of components is supposed after reaching equilibrium. If the standard deviation of the calculated and measured property obtained for the given chemical reactions is in the range of the experimental error, it is reasonable to assume that the structure of the electrolyte is given by the equilibrium composition determined by the calculated equilibrium constants. In addition, information on for example the thermal stability and the Gibbs' energy of the compounds which are present may be obtained. The task is solved by means of the material balance and using the thermodynamic relations valid for ideal solutions. In general, this approach may be used in the evaluation of those properties for which the ideal behaviour of the system is physically defined, e.g. for Gibbs' energy of mixing and molar volume. The procedure can be demonstrated on the calculation of equilibrium composition based on the measurement of density in the system A–B in which the intermediate compound AB is formed.

Let us consider 1 mol of mixture consisting of x_1 moles of component A and x_2 moles of component B. Since the partial thermal dissociation of AB must be taken into account, the degree of conversion of the reaction $A+B=AB$, α, has to be introduced. The equilibrium amounts of substances can be expressed as follows for $x_2 \leq 0.5$

$$n(A)=(1-2x_2+\alpha x_2)\ \text{mol}$$

$$n(B)=\alpha x_2\ \text{mol}$$

$$n(AB)=x_2(1-\alpha)\ \text{mol}$$

$$\text{Total}=(1-x_2+\alpha x_2)\ \text{mol}$$

and for the equilibrium mole fractions we can write

$$x_A=\frac{1-2x_2+\alpha x_2}{1-x_2+\alpha x_2},\quad x_B=\frac{\alpha x_2}{1-x_2+\alpha x_2},\quad x_{AB}=\frac{x_2(1-\alpha)}{1-x_2+\alpha x_2} \tag{3}$$

The degree of conversion of the reaction $A+B=AB$ is then given by the equilibrium constant

$$K=\frac{\alpha(1-2x_2+\alpha x_2)}{(1-\alpha)(1-x_2+\alpha x_2)}=\frac{\alpha_o^2}{1-\alpha_o^2} \tag{4}$$

where α_o is the degree of conversion to pure AB. For every value of the equilibrium constant we can calculate the equilibrium mole fractions of constituents for every composition. Recalculating the mole fractions $x(i)$ into mass fractions $w(i)$ and introducing them into the equation

$$\rho(\text{calc})=\left[\frac{w_A}{\rho_A}+\frac{w_B}{\rho_B}+\frac{w_{AB}}{\rho_{AB}}\right]^{-1} \tag{5}$$

which is based on the additivity of specific volumes, we get a set of density values for every chosen equilibrium constant. The accepted value of K is determined by

the condition

$$\sum_{i=1}^{n} [\rho_i(\text{calc}) - \rho_i(\text{exp})]^2 = \min \tag{6}$$

In the second approach, which finds application in real systems, the validity of the general Redlich–Kister type equation for the excess property is supposed. For the description of the composition dependence of the given property Y in the system, the following equation is then used (e.g. in a ternary system)

$$Y = \sum_{i=1}^{3} A_i.x_i \quad + \sum_{i\neq j}^{3} \sum_{i,j=1} x_i.x_j \sum_{n=0}^{n} B_{nij}.x_j^n + \sum_{a,b,c}^{m} C_m.x_1^a.x_2^b.x_3^c \tag{7}$$

The first term represents the additive behaviour, the second one the binary interactions and the third one the interaction of all three components. For the excess Gibbs' energy of mixing in the real solution the following equation may be supposed (e.g. for a ternary system)

$$\Delta G^{ex} = \sum_{i\neq j}^{3} \sum_{i,j=1}^{5} \sum_{n=1} A_{ijn}.x_i.x_j^n + \sum_{i\neq j\neq k}^{3} \sum_{i,j,k=1} B_{ijk}.x_i^a.x_j^b.x_k^c \tag{8}$$

In the case of transport properties, such as viscosity and electric conductivity, ideal behaviour is not physically defined, since we deal with scalar quantities which do not possess the total derivative. Thus, the simple additivity rule may not be used. However, these properties are thermally activated and the additivity of activation energies is allowed. Based on this idea the additivity of logarithms of these properties is often accepted as "ideal" behaviour. For the description of e.g. the viscosity in a three component system the following equation has been suggested

$$\eta = \eta_1^{x_1}.\eta_2^{x_2}.\eta_3^{x_3} \quad + \sum_{i\neq j}^{3} \sum_{i,j=1} x_i.x_j \sum_{n=0}^{k} A_{nij}.x_j^n + B.x_1^l.x_2^m.x_3^n \tag{9}$$

Coefficients of the regression Eqs. (7)–(9) are calculated using multiple linear regression analysis. Omitting the statistical non-important terms on the chosen confidence level and minimising the number of relevant terms we obtain a solution, which describes the concentration dependence of the property investigated with a standard deviation of the fit being of the same order as the experimental error. For statistically important binary and ternary interactions we look for appropriate chemical reactions and check their thermodynamic probability calculating their standard reaction Gibbs' energies. The reaction products are identified using the X-ray phase analysis and IR spectroscopy of quenched melts. Again we assume that the composition at high temperature is at least qualitatively conserved after quenching.

Interactions are mostly considered as chemical reactions between components.

However, van der Waals bonds and the formation of associates may not be excluded as interactions, even if they cannot be detected by spectroscopic measurements.

3. Deposition of molybdenum

An analysis of the literature data on the electrodeposition of molybdenum shows that several types of molten salts have been tested as electrolytes. On the basis of the electroactive species used, they can be divided into two main groups:

(1) halide systems containing either K_3MoCl_6 [5–9] or K_3MoF_6 [10] dissolved in alkali metal halides, mainly chlorides and fluorides;

(2) mixed systems containing oxide compounds of molybdenum, such as molybdenum oxide, MoO_3 [11–13], alkali metal molybdates [1,11,14–16] and $CaMoO_4$ [17]. Supporting electrolytes include: LiCl–KCl mixtures [12], sodium and lithium metaborates [11], KF–$Na_2B_4O_7$ [14], KF–$Li_2B_4O_7$ [1], KF–B_2O_3 [2,15], and $CaCl_2$–CaO [17].

Comparing the results of molybdenum electrodeposition from several types of electrolyte, it was confirmed in Ref. [2] that the process is most successful in electrolytes consisting of a mixture of alkali metal fluorides and boron oxide (or alkali metal borate) to which molybdenum oxide (or alkali metal molybdate) is added as the electrochemical active component.

The electrodeposition of molybdenum from binary MeF–Me_2MoO_4 mixtures does not occur [1–3,5–17]. However, a small addition (1 mol%) of boron oxide [1,2,11,14–16] or SiO_2 [3] to the electrolyte facilitates the electrodeposition of molybdenum. The presence of boron or silicon oxide most probably modifies the structure of the melt which results in changes in the cathode process.

3.1. Electrochemistry of molybdenum

The mechanism of the cathode process has been extensively studied in chloride-based electrolytes containing either Me_3MoCl_6 [18] or Me_2MoO_4 [12,17,19,20] as the electrochemically active species. For pure chloride electrolytes [18] the reduction of Mo(III) proceeds in a single three-electron irreversible step. It was found that the irreversibility of the process decreases with increasing temperature from 600 to 750 °C. However, chloride melts containing dissolved molybdenum(VI) oxide and alkali metal molybdates are found to be unsuitable for the electrodeposition of molybdenum because the primary product of the cathodic reaction is a molybdenum(III) oxide which is insoluble in the chloride melt.

Very promising electrolytes for the electrodeposition of molybdenum are melts of the system KF–K_2MoO_4–B_2O_3, especially when smooth, adherent molybdenum layers on metallic surfaces are desired [1].

The mechanism of molybdenum electrodeposition from potassium molybdate dissolved in a KF–B_2O_3 molten mixture was investigated by Guoxum and Defang [21]. The process proceeds in two consecutive charge transfer electrode reactions:

Mo(VI)→Mo(I)→Mo(0). The diffusion coefficient of Mo(VI) species in the melt is in the range $1.99–2.25 \times 10^{-5}\ cm^2 \cdot s^{-1}$.

The influence of B_2O_3 addition on molybdenum electrodeposition from molten K_2MoO_4 and KF–K_2MoO_4 electrolytes was studied in Ref. [22]. Fig. 1 shows the voltammetric curves recorded in a pure potassium molybdate melt and in the K_2MoO_4–B_2O_3 system with different boron oxide additions. On the voltammetric curve recorded in pure K_2MoO_4 (curve 1) only one electrochemical process is observed at a potential of approximately −1 V. This process represents electrodeposition of potassium on the cathode. The addition of a small amount of boron oxide to the basic melt causes significant changes in the shape of the voltammetric curves. A new expressive current peak starting at approx. −0.2 V appeared on the voltammetric curve (curves 2 and 3), with current depending on the B_2O_3 content in the melt. Similar behaviour was also observed using the KF–K_2MoO_4 system with SiO_2 additions.

On the basis of these results it is evident that the addition of oxides most probably causes changes in the ionic composition of the electrolyte, i.e. the kind of electroactive species from which molybdenum can be reduced. Changes in the ionic composition were studied using a physico-chemical and thermodynamic analysis (see below).

Makyta et al. [23] carried out chronopotentiometric and voltammetric measurements to determine the effect of electrolyte composition on the mechanism of molybdenum electrodeposition from KF–K_2MoO_4–B_2O_3 melts. The dissolution of potassium molybdate in molten KF–B_2O_3 mixtures is accompanied by chemical reactions between different boron-containing species such as $B_4O_7^{2-}$, BO_2^- and BF_4^- [24] and fluoride anions present at equilibrium in the basic KF–B_2O_3 melt. These chemical reactions most probably create new, molybdenum-containing electrochemically active species. Such multi-atomic species consisting of MoO_6 groups with boron as a central atom, present in the MoO_3-based glassforming melts, were described e.g. by Rawson [25].

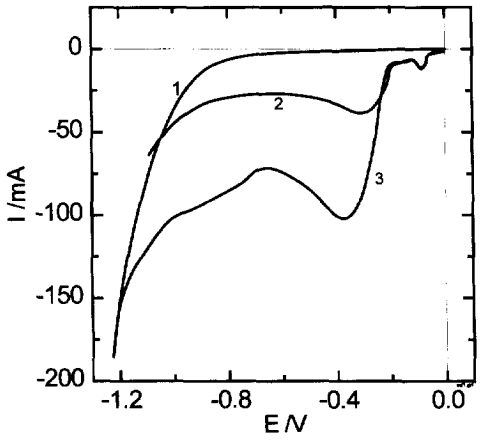

Fig. 1. Voltammetric curves in the KF–K_2MoO_4–B_2O_3 system. (1) Pure K_2MoO_4; (2) K_2MoO_4 + 2 mol% B_2O_3; (3) K_2MoO_4 + 5 mol% B_2O_3.

On the other hand, according to Makyta et al. [23], the reaction of potassium molybdate with fluoride anions creates electrochemically inactive molybdenum-containing species. These species are probably identical with those present in the molten $KF–K_2MoO_4$ mixture [26]. When all the boron-containing electrochemically active molybdenum species have been consumed, further dissolution of molybdate anions proceeds through formation of electrochemically inactive molybdenum species only.

In a series of chronopotentiometric measurements in melts containing 1.5 mol% B_2O_3 and more than 0.4 mol% K_2MoO_4, and in melts containing 3 mol% B_2O_3 and more than 1 mol% K_2MoO_4, Makyta et al. [23] observed only one wave on the chronopotentiometric curves. This observation together with previous results [2] indicate that the charge transfer electrode reduction of Mo(VI) from $KF–K_2MoO_4–B_2O_3$ melts proceeds in one six-electron step. These authors further claimed that the equilibrium chemical reaction between the various species in the melt, in accordance with the quantitative description of such a process published in Ref. [27], precedes probably this one-step electrode reduction. Based on a regression analysis of the chronopotentiometric data obtained at the two lowest K_2MoO_4 concentrations in the above two melts, and forcing the regression line to pass through zero, the diffusion coefficient of the electrochemically active molybdenum species was calculated to be 2.8×10^{-5} $cm^2 \cdot s^{-1}$. This value is in a good agreement with the value determined by Guoxum and Defang [21].

Similar electrolytic preparation of molybdenum coatings in the molten system $KF–K_2MoO_4–SiO_2$ has been investigated by Zatko et al. [28,29]. Coherent, smooth and well adhesive molybdenum layers were obtained on electrically conductive substrates in a relatively narrow composition region. The quality of the deposit depends on the silica content in the melt. The authors explain the positive role of SiO_2 in the molybdenum electrodeposition as being due to a change in the structure of the electrolyte and the formation in the melt of $[SiMo_{12}O_{40}]^{4-}$ heteropolyanions according to the reaction

$$12K_2MoO_4 + 7SiO_2 + 36KF = K_4[SiMo_{12}O_{40}] + 6K_2SiF_6 + 22K_2O \quad (10)$$

Such heteropolyanions are rather voluminous and thus much more polarizable. In the vicinity of the cathode in the electric double layer this anion is strongly polarised and finally disintegrated into smaller species, from which consecutive molybdenum deposition takes place. The X-ray diffraction analysis of the solid deposit on the top closure and furnace wall proved that the deposit thereon consists of pure K_2SiF_6, thereby supporting the formation of the above mentioned heteropolyanion. Unfortunately, the authors did not study the mechanism of the cathodic process in this system.

3.2. Structure of the $KF–K_2MoO_4–B_2O_3$ melts

In a number of papers measurement of different thermodynamic and transport properties of the $KF–K_2MoO_4–B_2O_3$ melts was done with the goal of clarifying their structure, i.e. the ionic composition on the basis of a complex physico-chemical analysis.

3.2.1. Subsystem $KF–K_2MoO_4$

In binary systems of alkali metal fluorides and other salts of alkali metals, such as sulphates, chromates, molybdates and tungstates, additive compounds such as Na_3FSO_4, K_3FCrO_4, K_3FWO_4, K_3TiF_7, K_3ZrF_7, etc., are formed. In the case of alkali metal chloride Cl^- may also be a ligand in the co-ordination sphere of the central atom. These compounds exhibit low symmetry of the complex anion most probably due to the repulsive forces between both anions. Owing to this effect and obviously a relatively high energetic state, such compounds often undergo a more or less extended thermal dissociation upon melting, in some cases they even melt incongruently. Evidence of such behaviour may be found e.g. in Refs. [30,31]. Into this group also belongs the compound K_3FMoO_4, formed in the system $KF–K_2MoO_4$.

The phase diagram of the binary system $KF–K_2MoO_4$ was studied by Schmitz-Dumont and Weeg [32], Mateiko and Bukhalova [33], and Julsrud and Kleppa [34]. The last authors also measured the enthalpies of mixing of this system. In this system is found the congruently melting addition compound K_3FMoO_4 with a melting point of 752 °C. This compound divides the system into two simple eutectic ones with the co-ordinates of the eutectic points of 29.2 mol% K_2MoO_4 and 720.4 °C in the subsystem $KF–K_3FMoO_4$ and 58.4 mol% K_2MoO_4 and 748.6 °C in the subsystem $K_3FMoO_4–K_2MoO_4$. From the flat course of the K_3FMoO_4 liquidus curve in this system it may be assumed that the addition compound undergoes considerable thermal dissociation. Upon melting the values obtained for the enthalpy of mixing indicate that the $KF–K_2MoO_4$ system deviates very little from ideal behaviour.

The phase diagram of the system $KF–K_2MoO_4$ (Fig. 2) was also later measured by Patarák et al. [35,36]. These authors showed that the addition compound K_3FMoO_4 melts at 751 °C. The co-ordinates of the individual eutectic points are as follows: 30 mol% K_2MoO_4 and 721 °C in the $KF–K_3FMoO_4$ subsystem and

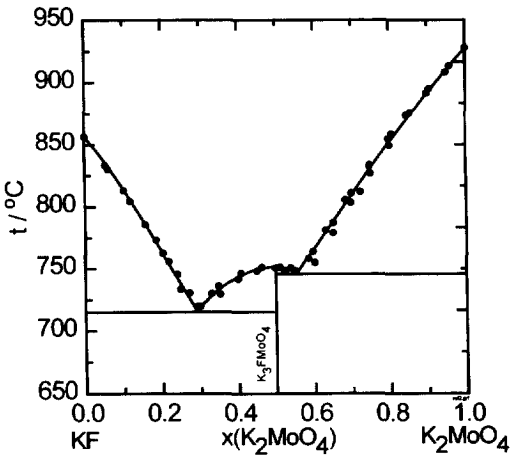

Fig. 2. Phase diagram of the $KF–K_2MoO_4$ system. Experiment [34,35] (●); calculated (———).

59 mol% K_2MoO_4 and 745 °C in the K_3FMoO_4–K_2MoO_4 subsystem. These values are very close to those obtained by Julsrud and Kleppa [34].

The densities of melts of the molten KF–K_2MoO_4 systems were measured in Ref. [26]. The density in this system increases monotonically with increasing content of K_2MoO_4. The concentration dependence of the molar volume of this system at 927 °C is described by the equation

$$V/\mathrm{cm}^3\ \mathrm{mol}^{-1} = 31.16 + 74.61x_{KF} - 8.70x_{KF}^2 + 5.76x_{KF}^3 \quad (11)$$

From the values of the excess molar volume it follows that the system shows only small deviations from ideal behaviour. The maximum deviation of 0.55% is attained at the concentration of $x(KF) = 0.75$. The formation of the congruently melting compound K_3FMoO_4 does not affect the molar volume course, since the excess molar volume at $x(KF) = 0.5$ is very close to zero. This indicates significant thermal dissociation of the addition compound.

The density data obtained in Ref. [26] were used in the calculation of the degree of thermal dissociation of the additive compound K_3FMoO_4. The result was also compared with the degree of thermal dissociation obtained from thermodynamic analysis of the phase diagram of the system investigated in Ref. [34] using the value of the enthalpy of fusion of K_3FMoO_4, taken from Ref. [37].

In Ref. [26] it was found that the degree of dissociation of K_3FMoO_4, obtained from analysis of the phase diagram, reaches a value $\alpha_o = 0.81$, confirming the pronounced thermal dissociation of K_3FMoO_4 during melting. Fig. 2 shows the experimentally determined [34] phase diagram for the KF–K_2MoO_4 system and the liquidus curves calculated for the value of the equilibrium dissociation constant $K_{dis,K_3FMoO_4} = 0.656$. The standard deviation of the fit was 6.8 °C. The fulfilment of the limiting laws for $x_i \rightarrow 1$ demonstrates the plausibility of the calculated equilibrium composition as well as the thermodynamic consistency of the experimental phase diagram. The value determined for the degree of dissociation of K_3FMoO_4 agrees very well with the value $\alpha_o(827\ °C) = 0.86$ determined by the analysis of the volume properties. Based on the dependence of the equilibrium dissociation constant on temperature, the enthalpy of dissociation $\Delta H_{dis,K_3FMoO_4} = 18.8\ \mathrm{kJ\ mol}^{-1}$ has also been calculated, representing a substantial part of the enthalpy of fusion $\Delta H_f = 58\ \mathrm{kJ\ mol}^{-1}$ [37].

The existence and structure of the complex anion $[FMoO_4]^{3-}$, however, may be a subject of discussion. Even though it cannot be identified by spectroscopic methods, obviously due to weak Mo–F or O–F bonds and probably also a short lifetime, this complex anion can be considered as an associate. Its acceptance is well-founded at least thermodynamically and serves as an useful example to understand the nature and behaviour of the investigated melts.

3.2.2. *Subsystem KF–B_2O_3*

The liquidus curve of KF in the KF–B_2O_3 system up to 20 mol% B_2O_3 was determined by Chrenková and Danek [38] and Patarák et al. [35,36] and is shown

in Fig. 3. According to the Gibbs' energy of the metathetical reaction

$$6KF_{(l)} + B_2O_{3(l)} = 3K_2O_{(s)} + 2BF_{3(g)} \quad (12)$$

$$\Delta G^0(827\ ^\circ C) = 940\ kJ\ mol^{-1}$$

the $KF–B_2O_3$ system should be the stable diagonal of the ternary reciprocal system K^+, $B^{3+}//F^-$, O^{2-}. However, a number of compounds are formed in this ternary reciprocal system. From the thermodynamic analysis of the liquidus curve of KF it follows, that the reaction

$$8KF_{(l)} + 7B_2O_{3(l)} = 3K_2B_4O_{7(l)} + 2KBF_{4(l)} \quad (13)$$

$$\Delta G^0(927\ ^\circ C) = -201.7\ kJ\ mol^{-1}$$

yielding two complex compounds KBF_4 and $K_2B_4O_7$, takes place in the melts. The presence of both compounds was also confirmed by means of the X-ray powder diffraction analysis and IR spectroscopy in the quenched samples. The positive deviation of the real liquidus curve from the theoretical one is most probably due to further polymerisation of the borate species.

The cryoscopic measurements of B_2O_3 in molten potassium fluoride were performed by Makyta [24]. He obtained the best fit of the experimental and theoretical liquidus curve for the reaction

$$32KF_{(l)} + 25B_2O_{3(l)} = 6KBO_{2(l)} + 9K_2B_4O_{7(l)} + 8KBF_{4(l)} \quad (14)$$

The last two originating compounds were confirmed both by the X-ray analysis and IR spectroscopy of quenched melts. $K_2B_4O_7$ is created preferentially with increasing content of B_2O_3 in the mixture. The presence of metaborate anions, however, was not detected, most probably due to its low concentration in the melt.

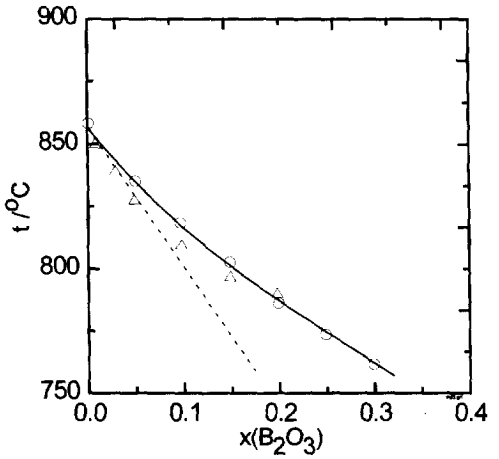

Fig. 3. Liquidus curve of KF in the $KF–B_2O_3$ system. Patarak et al. [35] (○); Chrenkova and Danek [38] (△); limiting course for two new particles (- - -).

The density of the $KF–B_2O_3$ system was measured in Ref. [19]. The density course in this system shows a minimum at 20 mol% B_2O_3. The concentration dependence of the molar volume at 827 °C was described by the second order polynomial

$$V/\mathrm{cm^3\ mol^{-1}} = 30.14 + 23.33x_{B_2O_3} - 47.23x^2_{B_2O_3} \quad (15)$$

Differentiating Eq. (15) and introducing into the equation

$$V_{B_2O_3} = V + x_{KF}\left[\frac{\partial V}{\partial x_{B_2O_3}}\right] \quad (16)$$

we obtain for the partial molar volume of B_2O_3 at a temperature of 827 °C the equation

$$V_{B_2O_3}/\mathrm{cm^3\ mol^{-1}} = 6.384 + 47.225x^2_{KF} \quad (17)$$

Following from this equation, for $x_{KF} \to 1$ the partial molar volume at 827 °C reaches the value $V_{B_2O_3} = 53.61\ \mathrm{cm^3\ mol^{-1}}$, being substantially higher than the molar volume of pure B_2O_3 ($V_{B_2O_3} = 44.62\ \mathrm{cm^3\ mol^{-1}}$), which indicates formation of larger ions. The formation of $K_2B_4O_7$ and KBF_4 according to Eq. (13) was confirmed in Refs. [24,39] using X-ray diffraction and IR spectroscopic analyses of the quenched melts.

3.2.3. *Subsystem $K_2MoO_4–B_2O_3$*

The liquidus curve of K_2MoO_4 was measured in the binary $K_2MoO_4–B_2O_3$ system only [35,36] (Fig. 4). The strong positive deviation from ideal behaviour is obvious. A similar course may be observed in systems with a strong tendency to immiscibility, or when more polymerised ions are formed in the liquid phase.

The ability of molybdates to form isopolyanions is well known. Moreover, in the

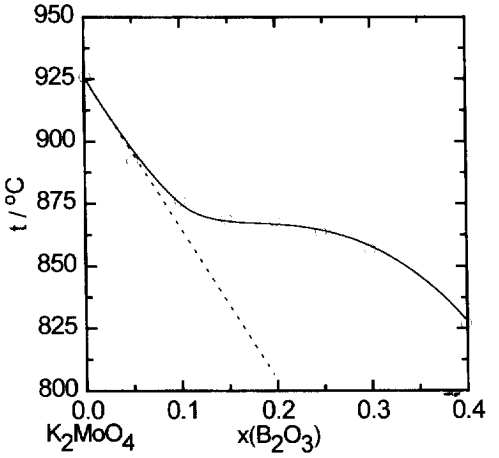

Fig. 4. Liquidus curve of K_2MoO_4 in the K_2MoO_4 B_2O_3 system. Experiment [35] (○); limiting course for two new particles (- - -); liquidus curve, if formation of $[BMo_6O_{24}]^{9-}$ heteropolyanions is considered (——).

presence of some foreign atoms, like B, Si, P, etc., they form heteropolyanions, in which the central foreign atom is co-ordinated by six, nine or twelve MoO_6 octahedra. The strong positive deviation of the liquidus curve may be caused by the formation of such heteropolyanions in the melt, according to the following equation

$$6K_2MoO_4 + 2B_2O_3 = K_9[BMo_6O_{24}] + 3KBO_2 \quad (18)$$

Taking into account this chemical reaction, and assuming a degree of conversion approximately equal to 1, the following relationship may be derived for the equilibrium mole fraction of K_2MoO_4 in the mixture

$$x(K_2MoO_4,eq) = \frac{4x(K_2MoO_4) - 3}{2x(K_2MoO_4) - 1} \quad (19)$$

where $x(K_2MoO_4)$ is the weighted mole fraction of K_2MoO_4. Using formally the theory of regular solutions, for the activity of K_2MoO_4 in the mixture, we can write [40]

$$a(K_2MoO_4,eq) = x(K_2MoO_4,eq).\exp\left[\frac{\Delta G^0}{RT}(1 - x(K_2MoO_4,eq)^2)\right] \quad (20)$$

where ΔG^0 is the standard Gibbs' energy of the chemical reaction Eq. (18) related to 1 mol K_2MoO_4 instead of the classical interaction parameter ω. The liquidus curve of K_2MoO_4, calculated according to Eq. (20) with the chosen value of $\Delta G^0 = -20$ kJ mol^{-1} is shown in Fig. 4 by the solid line. The value of the enthalpy of fusion of K_2MoO_4 was taken from Ref. [34]. The standard Gibbs' energy of reaction Eq. (18) should then be -120 kJ mol^{-1}. The very good agreement of the experimental and calculated liquidus curve confirms the above chemical reaction. This conclusion is confirmed also by the fulfilment of the limiting relation

$$\lim_{x(K_2MoO_4)\to 1}\left[\frac{da(K_2MoO_4)}{dx(K_2MoO_4)}\right] = 2 \quad (21)$$

Thus by the addition of one molecule of B_2O_3 into molten K_2MoO_4 two new particles, the anions $[BMo_6O_{24}]^{9-}$ and BO_2^-, are formed.

The density of the K_2MoO_4–B_2O_3 system [39] decreases monotonically with increasing content of B_2O_3. The concentration dependence of the molar volume of this system was described by a second order polynomial. Up to 20 mol% B_2O_3 the excess molar volume in this system is positive, while above this concentration the excess molar volume is negative. Differentiating the molar volume and introducing it into Eq. (16) the partial molar volume of B_2O_3 at the temperature of 827 °C is described by the following equation

$$V_{B_2O_3}/cm^3\ mol^{-1} = 3.875 + 41.171x^2_{K_2MoO_4} \quad (22)$$

and for $x(K_2MoO_4)\to 1$ $V(B_2O_3)$ is 45.05 cm^3 mol^{-1}. This value is surprisingly very close to the molar volume of pure B_2O_3. Both observations, the volume expansion up to 20 mol% B_2O_3 and the very good agreement of the partial molar volume of

B_2O_3 in dilute solutions in K_2MoO_4 with the partial molar volume of pure B_2O_3 may be explained by the formation of polymerised particles in the melt.

3.2.4. System $KF–K_2MoO_4–B_2O_3$

From the theoretical point of view, the melt systems $KF–K_2MoO_4–B_2O_3$ represent very little investigated electrolytes containing both classical ionic components and network forming ones. The possible chemical interactions between these are not well understood.

The $KF–K_2MoO_4–B_2O_3$ system is a considerably complicated subsystem of the quinary reciprocal system K^+, B^{3+}, $Mo^{6+}//F^-$, O^{2-}, in which a number of compounds are formed. The phase equilibrium in the $KF–K_2MoO_4–B_2O_3$ system was studied in Refs. [35,36]. The phase diagram of the ternary $KF–K_2MoO_4–B_2O_3$ system with up to 30 mol% B_2O_3, interesting from the viewpoint of electrochemical deposition of molybdenum, and constructed using the coupled analysis of thermodynamic and phase diagram data is shown in Fig. 5. The very extended plateau on the crystallisation surface of K_2MoO_4 shifts the boundary line with the primary crystallisation field of the additive compound K_3FMoO_4 to the KF corner, most probably due to formation of $[BMo_6O_{24}]^{9-}$ heteropolyanions in the ternary melts. The formation of $[BMo_6O_{24}]^{9-}$ heteropolyanions also indicates the excess Gibbs' energy of mixing of the system shown in Fig. 6. The enlarged shape of the crystallisation isotherms of K_2MoO_4 may also be due to the substitution of oxygen atoms of the co-ordination sphere of molybdenum in the $[BMo_6O_{24}]^{9-}$ heteropolyanions by fluoride. However, the existence of more highly polymerised heteropolyanions with Mo/B ratios of 9 or 12 may not be excluded.

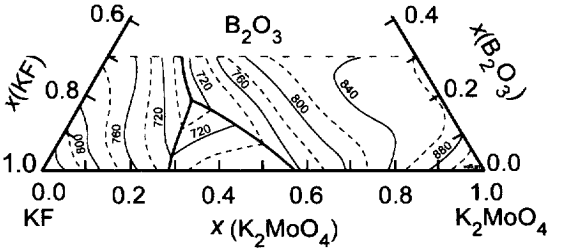

Fig. 5. Phase diagram of the $KF–K_2MoO_4–B_2O_3$ system.

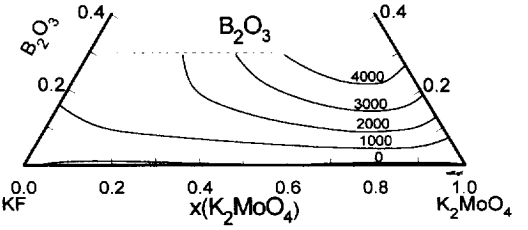

Fig. 6. Excess Gibbs' energy of mixing of the $KF–K_2MoO_4–B_2O_3$ system. Values are in J mol^{-1}.

The density of the $KF–K_2MoO_4–B_2O_3$ molten system was measured in Ref. [39]. For the concentration dependence of the molar volume at a temperature of 827 °C, the following equation was obtained

$$V/\mathrm{cm^3\ mol^{-1}} = 29.89x_{KF} + 89.50x_{K_2MoO_4} + 44.62x_{B_2O_3} + x_{KF}x_{K_2MoO_4} \times (8.50 - 5.28x_{K_2MoO_4}) + x_{KF}x_{B_2O_3}(11.92 - 53.22x_{B_2O_3}) - x_{K_2MoO_4}x_{B_2O_3}(81.31 + 102.51x_{B_2O}^{3}) + 110.29x_{KF}x_{K_2MoO_4}x_{B_2O_3} \quad (23)$$

The first three terms represent ideal behaviour, the next three, the interactions in the binary systems, and the last one the interaction of all three components. The coefficients were derived using the method of multiple linear regression analysis and omitting statistically non-important terms at the 0.99 confidence level. The standard deviation of the fit is 0.404 $cm^3\ mol^{-1}$. The different sign of the coefficients in the $KF–B_2O_3$ and $K_2MoO_4–B_2O_3$ systems indicates the different behaviour of B_2O_3 in KF and K_2MoO_4.

The excess molar volume of the $KF–K_2MoO_4–B_2O_3$ melts is shown in Fig. 7. From the figure it follows, that in this system a region of volume expansion exists with a maximum at 10 mol% B_2O_3 and 20 mol% K_2MoO_4, and a region of volume contraction with a maximum at 40 mol% B_2O_3 and 50 mol% K_2MoO_4.

The volume expansion region indicates the formation of larger ions according to Eq. (13), while in the volume contraction region the formation of $[BMo_6O_{24}]^{9-}$ heteropolyanions according to Eq. (18) and the probable further polymerisation of the melt, is assumed. The deviation from ideal behaviour is more pronounced in comparison with the boundary binary systems, which indicates stronger interaction of all three components. Such ternary interaction may be explained as the substitution of oxygen atoms in the co-ordination sphere of $[BMo_6O_{24}]^{9-}$ heteropolyanions by fluoride.

The viscosity of the $KF–K_2MoO_4–B_2O_3$ melts has been measured [41] using the computerised torsion pendulum method. The viscosity of the melts increases both with increased content of K_2MoO_4 and B_2O_3. Within experimental error the viscosity of the $KF–K_2MoO_4$ melts increases linearly with increasing K_2MoO_4 content. Taking into account this additive behaviour in the binary $KF–K_2MoO_4$ system and adopting

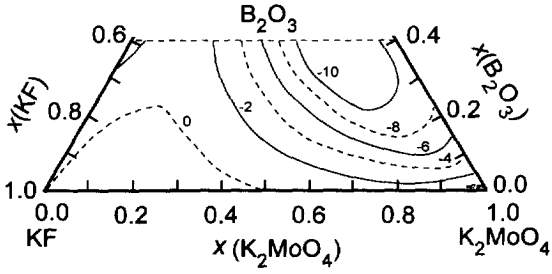

Fig. 7. Excess molar volume of the $KF–K_2MoO_4–B_2O_3$ system at $T = 827$ °C. Values are in $cm^3\ mol^{-1}$.

the formal value of 1000 Pa · s for the viscosity of pure boron oxide, the following final equation was obtained for the concentration dependence of the viscosity in the $KF–K_2MoO_4–B_2O_3$ ternary system at 877 °C

$$\begin{aligned}\eta/\text{mPa}\cdot\text{s} = {} & 1.28x_{KF} + 2.81x_{K_2MoO_4} + 999x_{B_2O_3} - x_{KF}x_{B_2O_3} \\ & \times (3317 - 3658x_{KF} + 1336x_{KF}^2) - x_{K_2MoO_4}x_{B_2O_3} \\ & \times (3242 - 3586x_{K_2MoO_4} + 1348x_{K_2MoO_4}^2) \\ & + x_{KF}x_{K_2MoO_4}x_{B_2O_3}(3214 + 4157x_{B_2O_3}) \end{aligned} \quad (24)$$

The standard deviation of the fit is 0.082 mPa · s. The viscosity of the ternary system at 927 °C is shown in Fig. 8. From the regression analysis it follows that the interaction in the binary $KF–K_2MoO_4$ system is statistically unimportant, compared with those in the $KF–B_2O_3$ and $K_2MoO_4–B_2O_3$ binary systems. The values of the standard deviations relate mostly to the viscosity of the ternary melts.

The viscosity of the ternary system melts increases very steeply with increasing content of boron oxide. This observation is, however, not surprising, because of the ability of boron oxide to polymerise. The formation of more voluminous $(B_4O_7)^{2-}$ and BF_4^- anions is obviously also increasing the viscosity of the melt. However, the increase of viscosity is higher than might be expected for the pure polycondensation of boron oxide. Evidently bigger particles than the boroxol rings are formed in the ternary system, especially near the $K_2MoO_4–B_2O_3$ boundary. According to conclusions based on phase equilibrium and density measurements these bigger particles are $[BMo_6O_{24}]^{9-}$ heteropolyanions formed in the melt according to Eq. (18). The statistically important ternary interaction, however, may also be ascribed to the entrance of fluorine atoms into the co-ordination sphere of molybdenum in the heteropolyanions.

From viscosity, as well as phase equilibrium and density measurements it is evident, that the $KF–K_2MoO_4–B_2O_3$ system is a very complex one. Beside the chemical reactions, the tendency of the melts to polymerise, especially in the region of higher contents of boron oxide, makes this system difficult to study. From physicochemical and thermodynamic analysis of the molten $KF–K_2MoO_4–B_2O_3$ and $KF–K_2MoO_4–SiO_2$ systems it follows that the formation of heteropolymolybdates containing boron, ($[BMo_6O_{24}]^{9-}$), and silicon, ($[SiMo_{12}O_{40}]^{4-}$), as a central atom is most probably responsible for the easy molybdenum deposition [42,43]. In addi-

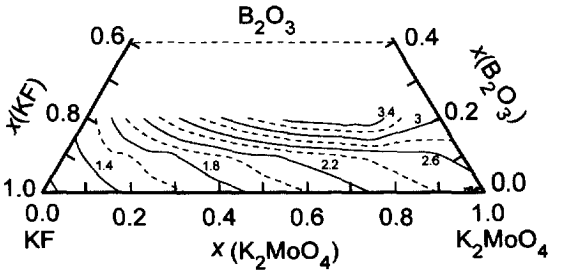

Fig. 8. Viscosity isotherms of the $KF–K_2MoO_4–B_2O_3$ system at $T = 1200$ K. Values are in mPa · s.

tion the entrance of fluorine atoms into the molybdenum co-ordination sphere in the heteropolyanions also lowers the symmetry and thus the electrochemical stability of such electroactive species.

4. Deposition of titanium and TiB_2

The electrochemical production, refining and electroplating of titanium and titanium diboride is a matter of scientific interest because of their use as advanced construction material in different technologies. Titanium diboride is especially considered to be a most promising material for inert cathodes in aluminium electrolysis [44] because it exhibits a high melting point, electronic conductivity, wettability by molten aluminium, and resistance towards chemical attack of aluminium and molten fluorides.

Electrolytes employed in the electrodeposition of titanium and/or titanium diboride consist of either oxygen-containing titanium and boron compounds [45–56], or binary halides of titanium and boron [52,57–68] as electrochemically active components. Mixtures of alkali halides serve as supporting electrolyte. Systems based on cryolite have also been tested [48,52,55,69]. Alkali chlorides, in comparison to fluorides, exhibit some obvious advantages as far as price, low corrosion of construction materials and easy separation of the product from the cathodic deposit containing solidified electrolyte.

4.1. Electrochemistry of titanium

Inman and White [70] report a comprehensive literature review up to 1977 of the electrochemistry of titanium in molten salt electrolytes and there is a more recent report by Girginov et al. [71]. The following conclusions may be drawn concerning the mechanism of the cathodic process in different types of electrolytes.

The chemical nature of the anionic environment and the nature of the alkali metal cation, play an important role in the mechanism of cathodic reduction.

In all-chloride melts, the reduction of Ti(III) to metallic titanium proceeds in general in two steps [69,71]: Ti(III)→Ti(II)→Ti(0). According to Chassaing et al. [59,60], the following equilibria take place in NaCl–KCl–$TiCl_3$ melts

$$TiCl_6^{3-} = TiCl_4^{-} + 2Cl^{-} \quad (25)$$

$$TiCl_6^{3-} = 0.5Ti_2Cl_9^{3-} + 1.5Cl^{-} \quad (26)$$

With decreasing scan rate the voltammetric peak corresponding to the first reduction step Ti(III)→Ti(II) gradually disappears, eventually merging into the next peak ascribed to the reduction Ti(II)→Ti(0) and the process apparently becomes a single-step one. In electrolytes based on CsCl the $TiCl_6^{3-}$ complex ions become more stable compared with those of NaCl and KCl due to the lower polarising effect of Cs^+. Consequently, Ti(III) is reduced to titanium metal in a single step Ti(III)→Ti(0) [58].

In chloride–fluoride mixed electrolytes a partial substitution of the large chloride ligands in the $TiCl_6^{3-}$ anion by the smaller fluoride ones with formation of $TiCl_{6-x}F_x^{3-}$ anions also causes a change in the mechanism of Ti(III) reduction. In the NaCl–KCl–NaF–$TiCl_3$ melts the single step reduction

$$TiCl_4F_2^{3-} + 3e^- = Ti + 4Cl^- + 2F^- \quad (27)$$

takes place [69], and is a simple irreversible charge transfer reaction which is not complicated by any preceding chemical reaction. With decreasing concentration of TiF_6^{2-} in the NaCl–KCl–K_2TiF_6 melts the composition of the Ti(IV) complexes changes from $TiF_x^{(x-4)-}$ through $TiF_xCl_y^{(x+y-4)-}$ to $TiCl_y^{(y-4)-}$ [58].

The mechanism of Ti(IV) reduction in all-fluoride melts was studied e.g. by Sequeira [63], De Lepinay et al. [64,65] and Makyta et al. [56,67]. According to these authors the mechanism of the cathode process in the LiF–KF–K_2TiF_6 or LiF–NaF–KF–K_2TiF_6 melts can be described by the sequence Ti(IV)→Ti(III)→Ti(0).

The influence of the melt composition on the deposition of titanium from the K_2TiF_6 melt was studied by Makyta et al. [22,72]. The essential results of this work are summarised in Fig. 9. From comparison of the cathodic part of the voltammetric curves obtained in pure K_2TiF_6 (curve 1) and those obtained in the KF–K_2TiF_6 and KCl–K_2TiF_6 mixtures (curves 2–4) substantial changes occur when KF or KCl is added to the pure K_2TiF_6. As mentioned above, the reduction of Ti(IV) to titanium metal in the all-fluoride and chloride–fluoride melts proceeds in two electrochemical consecutive reduction steps, Ti(IV)→Ti(III)→Ti(0). These two reduction steps are clearly visible in all recorded curves, the first starting at approximately −0.2 V and the second starting at approximately −1.5 V. The values of the individual peak currents, representing the above titanium reduction steps, increase with increasing content of potassium chloride in the melt (Fig. 9). Similar changes were also observed on voltammetric curves when KF was added to K_2TiF_6. In spite of

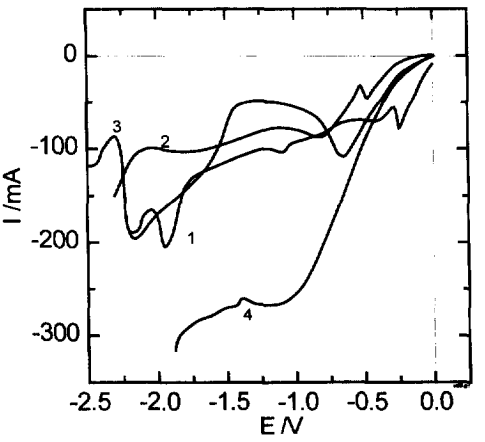

Fig. 9. Voltammetric curves in the K_2TiF_6–KCl system. (1) K_2TiF_6; (2) K_2TiF_6+5 mol% KCl; (3) K_2TiF_6+50 mol% KCl; (4) K_2TiF_6+90 mol% KCl.

the fact that titanium may also be deposited from pure K_2TiF_6, most probably due to the presence of KF impurities, the addition of either KF or KCl significantly increases the peaks current corresponding to titanium reduction.

On the basis of these results, the addition of KF or KCl is most probably changing the ionic composition of the electrolyte, i.e. the character of the electroactive species, thereby enhancing the electroreduction of titanium. The changes in ionic composition were studied using physico-chemical and thermodynamic analysis (see below).

On the other hand, according to Girginov et al. [71], the one stop four-electron reduction Ti(IV)→Ti(0) is the most accepted mechanism in oxide electrolytes. The mechanism of TiB_2 electrodeposition from LiF–KF–B_2O_3–TiO_2 melts was also studied by Makyta and Utigard [56]. These melts are very suitable electrolytes especially for the preparation of fine uniform TiB_2 powders with an average grain size up to 5 μm. The mechanism of TiB_2 synthesis is rather complex. On the basis of the electrochemical measurements either the electrochemical or electro-metallothermal mechanisms take place depending on the potential applied.

Hence, as in the electrodeposition of molybdenum, the ionic structure of the electrolyte, especially the kind of electroactive species, is the most important factor influencing the electrodeposition of titanium. Since titanium is reduced mainly from Ti(IV) complex-containing anions, the thermochemical stability of these compounds also plays a substantial role in high temperature electrochemical applications.

4.2. *Structure of the KF–KCl–KBF_4–K_2TiF_6 melts*

Melts of the quaternary KF–KCl–KBF_4–K_2TiF_6 system are very suitable electrolytes in the electrochemical synthesis of TiB_2, especially when coherent coatings on metallic bases have to be prepared [66]. In a series of papers the structure of these melts was investigated by means of complex physico-chemical analysis. The measurement of different thermodynamic and transport properties was performed and the structure of these melts was derived. We will analyse the important boundary ternary systems individually.

4.2.1. *Subsystem KF–KCl–KBF_4*

In addition to the electrochemical TiB_2 coating application mentioned above, the KF–KCl–KBF_4 molten system is also interesting as a possible electrolyte for the electrochemical boriding of steels [73,74]. The interaction of components and the chemical reactions possible taking place in the melt, affect the ionic composition, thus determining the kind of electroactive species. The appropriate choice of the electrolyte composition may prevent the formation of volatile compounds, like BCl_3, which leads to undesirable exhalations and lowers the efficiency of the process.

The phase diagrams of the boundary binary systems of the KF–KCl–KBF_4 ternary system have been studied [75–78]. All three binary systems are simple eutectics. In the phase diagram of the KCl–KBF_4 system determined in Ref. [75], formation of the congruently melting compound $11 \cdot KBF_4 \cdot KCl$ was suggested. However, the existence of this compound was not confirmed in later investigations [76,77].

The phase diagram of the KF–KCl–KBF_4 ternary system was measured in

Ref. [79]. The system is a simple eutectic with eutectic point co-ordinates of 19.2 mol% KF, 18.4 mol% KCl and 61.4 mol% KBF_4 and a temperature of eutectic crystallisation of 422 °C.

Among the physico-chemical properties, the density and conductivity of the KF–KCl binary system [80], the density of pure KBF_4 [81], as well as the conductivity of the KF–KBF_4 binary system [82] have been measured. However, the conductivity data of the latter system seems unreliable. The density of the ternary KF–KCl–KBF_4 system was measured in Ref. [83], the electrical conductivity in Ref. [84] and the viscosity in Ref. [85].

The reactions of potassium tetrafluoroborate in molten alkali chlorides were investigated in Ref. [86] using the cryoscopic method. The main aim of this work was to study the stability of the BF_4^- anion in the presence of Cl^- anions and different cationic environments. KBF_4 is unstable in molten LiCl and decomposes with formation of gaseous BCl_3. In molten NaCl the exchange reaction between KBF_4 and the Cl^- anions with the formation of $KBCl_4$ only proceeds at very low concentrations of KBF_4 while no reaction occurs in molten KCl, the BF_4^- anion is relatively stable up to approx. 900 °C. The experimental results were supported by thermodynamic calculations.

From the results of the physico-chemical analysis [79,83–85] deviations from ideal behaviour were observed in all the boundary binaries as well as in the ternary system. Since the system investigated has a common cation, the observed deviations from ideal behaviour must be a consequence of the anionic interaction only. The interaction of components may be of a different origin. Primarily, a different interaction character must be present in the boundary binaries KF–KBF_4 and KCl–KBF_4.

In pure KBF_4 melt, BF_4^- tetrahedra tend to link, forming relatively weak B–F–B bonds. The strength of this bond depends strongly on temperature. By introducing F^- ions into the KBF_4 melt by addition of KF, the B–F–B bridges break, lowering the viscosity and leading to a negative deviation from ideal behaviour in the KF–KBF_4 system. In addition there is mixing between the small F^- anions with the relatively large BF_4^- anions. In systems of this type the deviation from additivity is proportional to the fractional difference in the radii of the different anions [87]. Therefore a relatively large deviation from ideality may be achieved, confirmed by density [83], conductivity [84] or viscosity [85] measurements.

An opposite interaction effect takes place in the KCl–KBF_4 system where the mixing of two relatively large and polarizable BF_4^- and Cl^- anions occurs. As in alkali metal chloride, bromide and iodide systems with a common cation, no important deviations from additivity were found [78,87]. Such behaviour was also confirmed in the KCl–KBF_4 system by density [83], conductivity [84] and viscosity [85] measurements. On the other hand, introducing Cl^- ions into the KBF_4 melt, the exchange of fluoride atoms in BF_4^- tetrahedra by chloride takes place according to the general scheme

$$BF_4^- + nCl^- \Leftrightarrow [BF_{4-n}Cl_n]^- + nF^- \tag{28}$$

and $[BF_{4-n}Cl_n]^-$ mixed anions may be present. Consequently, the lower stability of

the B–Cl–B bridges and the lower concentration of B–F–B leads to negative deviations of the properties in the $KCl–KBF_4$ system. This explanation is also supported by the asymmetric course of the excess viscosity curve, which is due to reaction Eq. (28) shifted to the right side in the region of high concentration of KBF_4.

In the KF–KCl binary system the origin of the negative deviations in properties may be sought in the mutual influence of the degree of dissociation of the components, described in detail in the dissociation model of the electric conductivity of molten salt mixtures [87].

The negative deviations, found in the $KF–KCl–KBF_4$ ternary system, obviously have the same origin as was described for boundary binary systems. Following from the course of the excess molar Gibbs' energy of mixing (Fig. 10), the excess molar volume (Fig. 11), the excess molar conductivity (Fig. 12) and the excess viscosity (Fig. 13) in the system investigated, the maximum interaction effect is localised near the $KF–KBF_4$ boundary.

The anionic interaction according to reaction Eq. (28) was confirmed by infrared spectroscopy. The IR spectra of KBF_4 and that of the quenched molten KBF_4–KCl (1:1 mole ratio) mixture are shown in Fig. 14. Except for the 600–900 cm^{-1} region, the mid infrared spectra of both samples are almost identical. In agreement with the earlier study of the alkali metal tetrafluoroborates [88], common vibrations can be assigned to crystalline KBF_4. Significant differences have been observed only in the 600–900 cm^{-1} region. It is obvious that besides the $\nu(1)$ vibration corresponding to KBF_4, the quenched molten KBF_4–KCl mixture produces two additional peaks at 760 and 796 cm^{-1} with a shoulder at 770 cm^{-1}. These peaks arise due to different B–F and B–Cl valence vibrations in the $[BF_{4-n}Cl_n]^-$ anions. The substitution of fluorine atoms by chlorine in the co-ordination sphere of the BF_4^- anion in molten $KF–KCl–KBF_4$ mixtures was thus confirmed. However, the

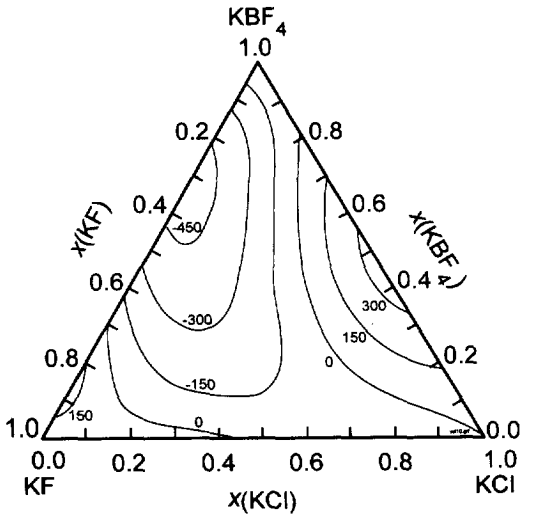

Fig. 10. Excess Gibbs' energy of mixing in the $KF–KCl–KBF_4$ system. Values are in J mol^{-1}.

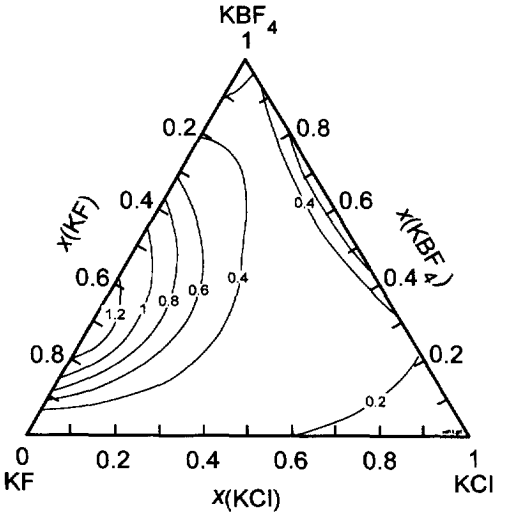

Fig. 11. Excess molar volume of the KF–KCl–KBF_4 system at $T=1100$ K. Values are in $cm^3\ mol^{-1}$.

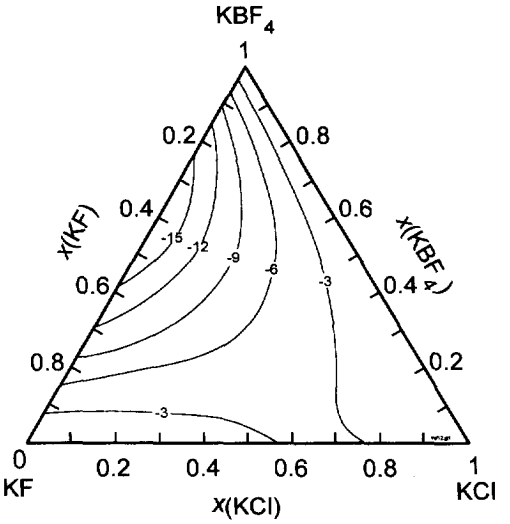

Fig. 12. Excess molar conductivity of the KF–KCl–KBF_4 system at $T=1100$ K. Values are in $S\ cm^2\ mol^{-1}$.

type of mixed anion was not determined either by physico-chemical analysis or by spectroscopy.

4.2.2. Subsystem KF–KCl–K_2TiF_6

As mentioned in Section 3.2.1, in alkali metal fluoride and transition metal fluoride binary systems complex compounds like K_3TiF_7, K_3ZrF_7, K_3ZrF_6Cl, etc., are

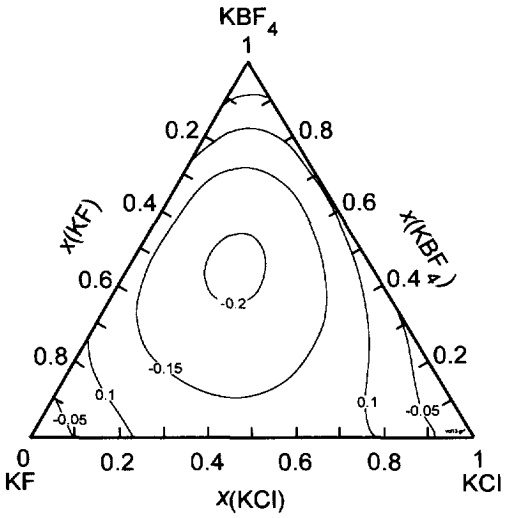

Fig. 13. Excess viscosity of the KF–KCl–KBF_4 system at $T=1100$ K. Values are in mPa · s.

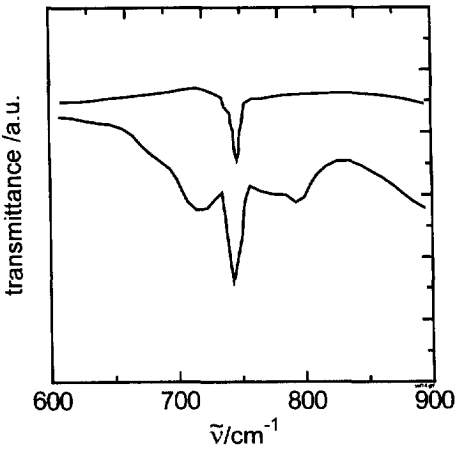

Fig. 14. IR spectra of quenched KBF_4 and KBF_4–KCl melts.

formed. These compounds often at melting undergo a more or less extended thermal dissociation, in some cases they even melt incongruently [89]. The thermal stability and degree of thermal dissociation of several complex compounds Me_3XF_7 (Me = Li, Na, K; X = Ti, Zr, Hf), have been calculated on the basis of the known phase diagrams for the MeF–Me_3XF_7 systems [90].

From the calculated values for the degree of dissociation the thermal stabilities of the Me_3XF_7 compounds depend on the chemical nature of both the central transition metal and the alkali metal cation present. The thermal stability increases with increasing size of the transition metal, obviously due to the steric and conse-

quently the energetic relations. The thermal stability of the complex anion is also influenced by the size of the ligands present. The substitution of the fluorine atom in the co-ordination sphere of the transition metal by chlorine leads to a decrease of the thermal stability of the compound.

The influence of the alkali metal cation present on the thermal stability of Me_3XF_7 follows the general trend of alkali metal compounds, concerning e.g. their melting temperatures and other properties. With the exception of the lithium compounds the thermal stability decreases with increasing electronegativity of the alkali metal obviously due to the lowering of the electrostatic forces between the complex anion and the alkali cation.

The thermal stability of the compounds investigated is also closely related to the symmetry of the co-ordination sphere. From the proposed crystal structure of the Me_3XF_7 compounds [91–93] the XF_7^{3-} complex anion is co-ordinated by eight fluorine atoms forming a flat tetragonal prism. Such a configuration is in accordance with the relatively high thermal stability of the heptafluorozirconates and heptafluorohafniates. Unfortunately, the crystal structures of the less stable potassium heptafluorotitanate and their hexafluoro–chloro derivatives are not known. The latter probably have the lower symmetry.

The phase diagram of the $KF–K_2TiF_6$ system has been studied [94]. The congruently melting K_3TiF_7 compound with melting temperature of 1048 K is formed. The zero value of the tangent to the K_3TiF_7 liquidus curve at $x(K_2TiF_6)=0.5$ indicates that this compound undergoes considerable thermal dissociation upon melting. The degree of dissociation calculated on the basis of the experimentally determined phase diagram, $\alpha_o=0.64$ [95], is in a very good accordance with the values obtained from the density data, $\alpha_o(1000\,K)=0.6$ and $\alpha_o(1100\,K)=0.7$ [96]. From the temperature dependence of the degree of dissociation the dissociation enthalpy $\Delta H_{dis.K_3TiF_7}=52.4$ kJ mol^{-1} was calculated. This value represents a substantial part of the enthalpy of fusion $\Delta H_{f.K_3TiF_7}=56.0$ kJ mol^{-1}.

The phase diagram of the $KCl–K_2TiF_6$ system was studied in Ref. [97]. As in the previous system, a congruently melting compound K_3TiF_6Cl with a melting temperature of 964 K is formed. K_3TiF_6Cl also undergoes considerable thermal dissociation upon melting with $\alpha_o=0.78$ calculated on the basis of phase equilibria, with good agreement with the density measurements $\alpha_o(1000\,K)=0.72$ and $\alpha_o(1100\,K)=0.81$ [96]. The dissociation enthalpy was found to be $\Delta H_{dis.K_3TiF_6Cl}=46.6$ kJ mol^{-1}, again being a substantial part of the enthalpy of fusion $\Delta H_{f.K_3TiF_6Cl}=52.9$ kJ mol^{-1}.

The behaviour of K_2TiF_6 in dilute alkali metal halide solutions has been studied by Danek et al. [98]. In molten LiCl as well as in the LiCl–KCl eutectic mixture the substitution of fluorine in TiF_6^{2-} by chlorine takes place, while in the LiF–LiCl eutectic mixture this reaction does not occur. In molten NaCl and KCl no substitution reaction between TiF_6^{2-} and Cl^- anions takes place. The experimental results are in good agreement with thermodynamic calculations.

The phase diagram of the ternary $KF–KCl–K_2TiF_6$ system has been studied [99]. Two congruently melting compounds, K_3TiF_7 and K_3TiF_6Cl, are formed in this system (Fig. 15). These compounds also exhibit an extended thermal dissociation

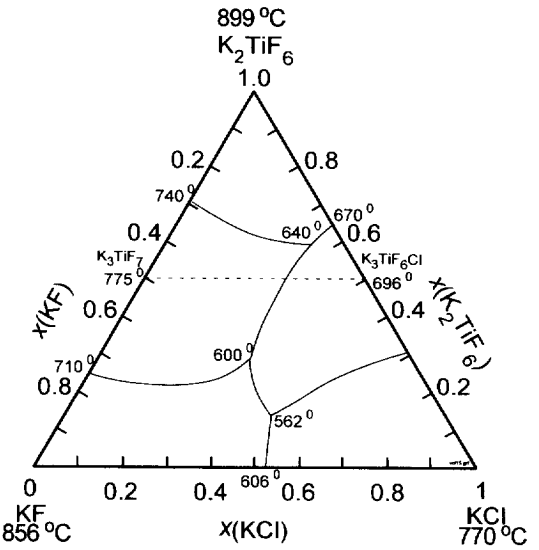

Fig. 15. Phase diagram of the KF–KCl–K_2TiF_6 system.

according to

$$K_3TiF_7 = KF + K_2TiF_6 \tag{29}$$

$$K_3TiF_6Cl = KCl + K_2TiF_6 \tag{30}$$

This behaviour was also confirmed by measurements of the volume [98] and viscosity [100] properties of this system.

The density of the KF–KCl–K_2TiF_6 melts is influenced mostly by the KCl component, which strongly decreases the density of the melts. The dependence of the excess molar volume on composition was calculated using regression analysis and the following equation at $T = 1100$ K was obtained

$$V^E/\text{cm}^3\ \text{mol}^{-1} = 0.763 x_{KF} x_{KCl} + x_{KF} x_{K_2TiF_6}(2.236 - 2.956 x_{K_2TiF_6}) - x_{KCl} x_{K_2TiF_6}(21.817 - 68.506 x_{K_2TiF_6} + 54.552 x^2_{K_2TiF_6}) \tag{31}$$

with a standard deviation of $\sigma = 0.047\ \text{cm}^3\ \text{mol}^{-1}$.

In Fig. 16 the excess molar volume of the KF–KCl–K_2TiF_6 melts at 1100 K is shown, indicating only a small deviation from ideal behaviour. The maximum deviation is $-1.5\ \text{cm}^3\ \text{mol}^{-1}$ which represents 2.23% of the molar volume for the respective melt. The formation of K_3TiF_7 and K_3TiF_6Cl compounds does not substantially affect the volume properties. This indicates that either these compounds dissociate in the melt to a considerable degree, or the volumes of the TiF_6^{2-}, TiF_7^{3-} and TiF_6Cl^{3-} anions are fairly similar. No ternary interaction was found.

The viscosity of the ternary melts increases from KCl through KF and from the

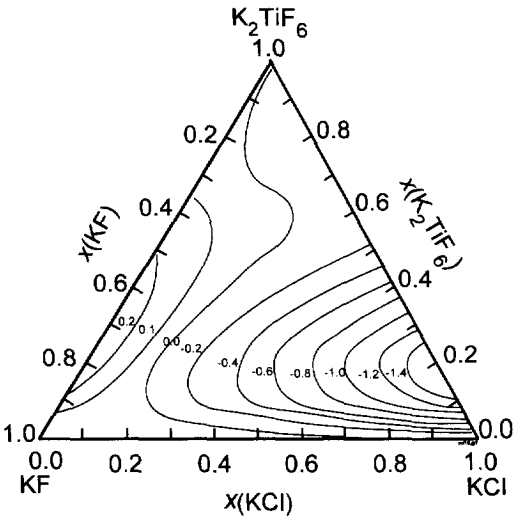

Fig. 16. Excess molar volume of the KF–KCl–K_2TiF_6 system at $T=1100$ K. Values are in $cm^3\ mol^{-1}$.

binary system KF–KCl to K_2TiF_6. The higher viscosity of KF compared with that of KCl is probably due to the presence of F–F bridges in the KF melt.

Adopting the additivity of logarithms of viscosity as the ideal behaviour [101,102], for the description of viscosity in the three-component system, the following equation was obtained

$$\begin{aligned}\ln \eta = [&-2.438x_{KF} - 2.777x_{KCl} - 1.948x_{K_2TiF_6} \\ &+ \frac{1}{T}(3068x_{KF} + 3002x_{KCl} + 3641x_{K_2TiF_6})] \\ &-[(1.000x_{KF}x_{KCl} + 5.728x_{KF}x^3_{K_2TiF_6} + 11.20x_{KCl}x^3_{K_2TiF_6}) \\ &+ \frac{1}{T}(620.1x_{KF}x_{KCl} + 8072x_{KF}x^3_{K_2TiF_6} + 13390x_{KCl}x^3_{K_2TiF_6})] \\ &+ 21.20x_{KF}x^2_{KCl}x^3_{K_2TiF_6} \end{aligned} \quad (32)$$

with a standard deviation of fit $\sigma = 7.1 \times 10^{-4}$. The first term represents the ideal behaviour, the next the interactions in the binary systems, which are dependent on temperature, while the last term describes the interaction of all three components as temperature-independent. The validity of Eq. (32) is in the temperature interval 700–1300 K.

The course of the excess viscosity in the binary systems is shown in Fig. 17. In the KF–KCl binary system negative deviations from ideal behaviour were observed, perhaps due to non-random mixing of the anions.

In the binary KF–K_2TiF_6 system the TiF_7^{3-} anion is formed, increasing the viscosity of the melt. Therefore, the excess viscosity in this system is positive. Similar

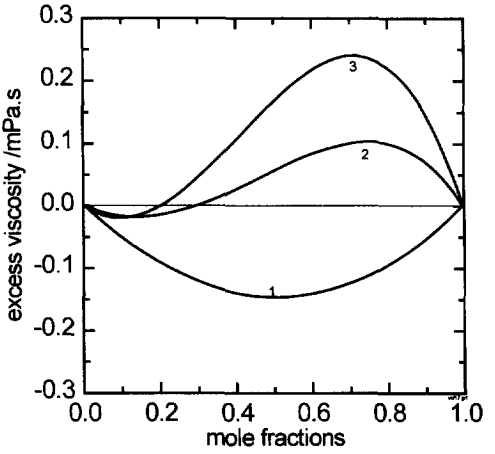

Fig. 17. Excess viscosity of the boundary binary systems at $T=1100$ K. (1) KF–KCl; (2) KCl–K_2TiF_6; (3) KF–K_2TiF_6.

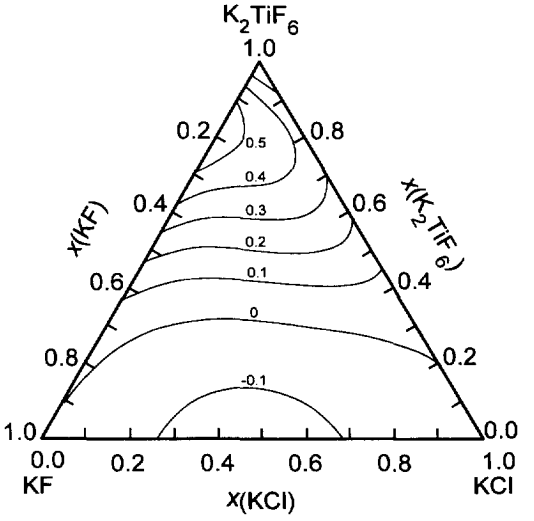

Fig. 18. Excess viscosity of the KF–KCl–K_2TiF_6 system. Values are in mPa·s.

conclusions may be drawn for the KCl–K_2TiF_6 system, where the anion TiF_6Cl^{3-}, formed in this system, also increases the viscosity.

The iso-excess-viscosity lines of the ternary KF–KCl–K_2TiF_6 system (Fig. 18) reveal the formation of TiF_7^{3-} and TiF_6Cl^{3-} in this ternary system. From the positive value of the statistically important ternary interaction, described by the last coefficient in Eq. (32), the degrees of their thermal dissociation in the ternary system decrease.

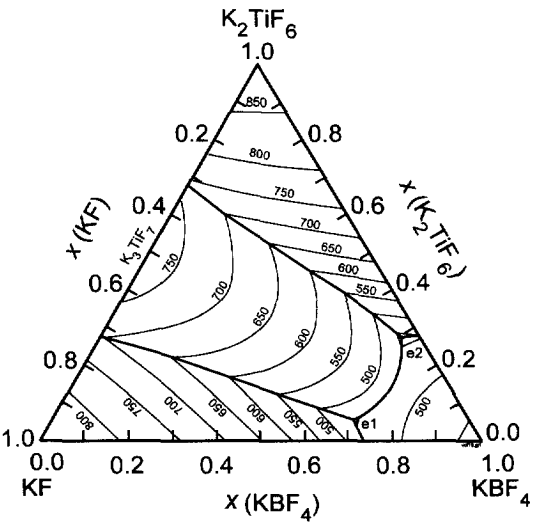

Fig. 19. Phase diagram of the $KF–KBF_4–K_2TiF_6$ system.

4.2.3. Subsystem $KF–KBF_4–K_2TiF_6$

The coupled analysis of the thermodynamic and measured phase diagram data has been performed [103]. The phase diagram of the $KF–KBF_4–K_2TiF_6$ system is shown in Fig. 19. Four crystallisation fields are present in the phase diagram corresponding to the primary crystallisation of KF, KBF_4, K_2TiF_6 and the intermediate compound K_3TiF_7. The calculated co-ordinates of the two ternary eutectic points are:

e_1: 26 mol% KF, 69 mol% KBF_4, 5 mol% K_2TiF_6, $t_{e1} = 448$ °C;

e_2: 4 mol% KF, 69 mol% KBF_4, 27 mol% K_2TiF_6, $t_{e2} = 440$ °C.

The probable inaccuracy in the calculated ternary phase diagram is ± 11.5 °C.

For the molar excess Gibbs' energy of mixing the following equation was obtained

$$\begin{aligned}\Delta G^{E}/\mathrm{J\,mol^{-1}} = {} & x_{KF}x_{KBF_4}(3569 - 15930x_{KBF_4} + 8347x_{KBF_4}^2) \\ & - x_{KF}x_{K_2TiF_6}(13319 + 14895x_{K_2TiF_6} - 26989x_{K_2TiF_6}^2) \\ & - x_{KBF_4}x_{K_2TiF_6}(3688 - 11864x_{K_2TiF_6}) \\ & - 26897x_{KF}x_{KBF_4}x_{K_2TiF_6} \end{aligned} \quad (33)$$

The first term represents the molar excess Gibbs' energy of mixing in the binary $KF–KBF_4$ system, the second in the binary $KF–K_2TiF_6$ system and the third in the binary $KBF_4–K_2TiF_6$ system. The last term represents the interaction contribution in the ternary system. The molar excess Gibbs' energy of mixing in the ternary $KF–KBF_4–K_2TiF_6$ system is shown in Fig. 20.

The phase diagram of the boundary $KF–KBF_4$ system is shown in Fig. 21. A

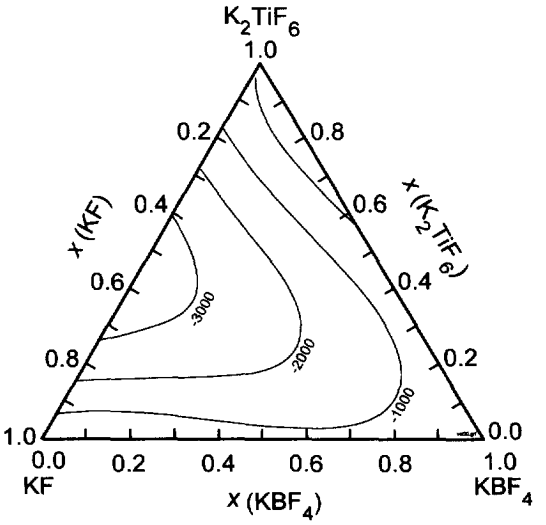

Fig. 20. Excess Gibbs' energy of mixing in the $KF–KBF_4–K_2TiF_6$ system. Values are in J mol^{-1}.

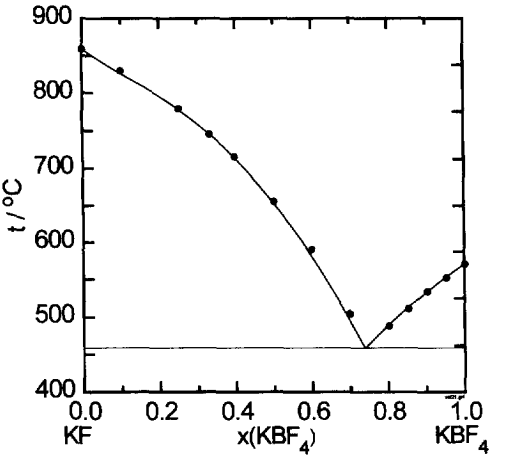

Fig. 21. Phase diagram of the $KF–KBF_4$ system.

third order polynomial was obtained for the concentration dependence of the molar excess Gibbs' energy of mixing in this system. The calculated co-ordinates of the eutectic point 74 mol% KBF_4 and 460 °C agree well with those given in Ref. [76]. The significant inflex course of the liquidus curve of KF in the region of low KBF_4 concentration is most probably due to the decreasing stability of KBF_4 with increasing temperature. At higher temperatures KBF_4 probably decomposes with the formation of gaseous BF_3.

The phase diagram of the boundary $KF–K_2TiF_6$ system is shown in Fig. 22. A

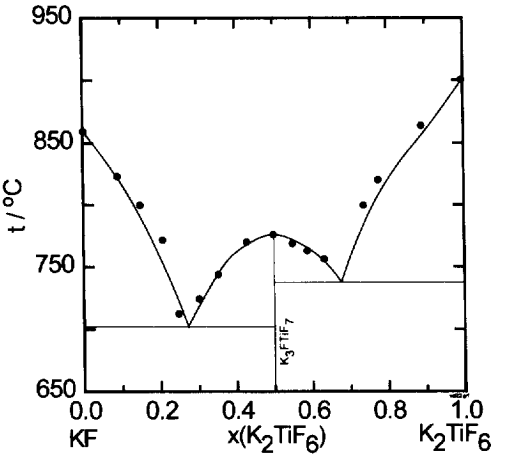

Fig. 22. Phase diagram of the $KF–K_2TiF_6$ system.

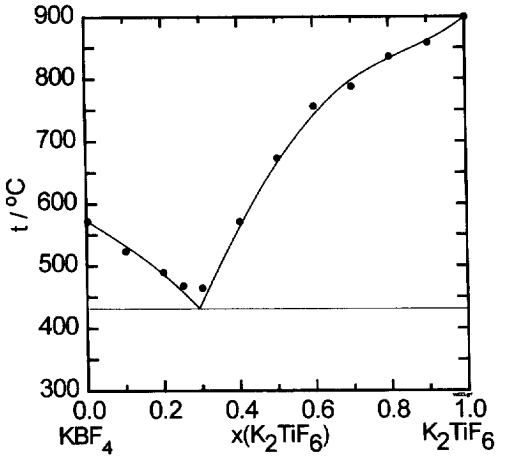

Fig. 23. Phase diagram of the $KBF_4–K_2TiF_6$ system.

third order polynomial for the molar excess Gibbs' energy of mixing was obtained. The co-ordinates of both eutectic points (e_1: 28 mol% K_2TiF_6, 701 °C; e_2: 68 mol% K_2TiF_6, 738 °C) differ from those given in Ref. [104], probably due to the appreciable inaccuracy in the determination of the liquidus temperature in Ref. [104].

Similar results were also obtained for the boundary $KBF_4–K_2TiF_6$ system. The phase diagram is shown in Fig. 23. The $KBF_4–K_2TiF_6$ system is a simple eutectic with the co-ordinates of the eutectic point 28 mol% K_2TiF_6 and 448 °C. As in the $KF–KBF_4$ system, the significant inflex course of the K_2TiF_6 liquidus curve is most probably due to the decomposition of KBF_4 and escape of gaseous BF_3.

The volume properties of the ternary $KF–KBF_4–K_2TiF_6$ system melts were studied

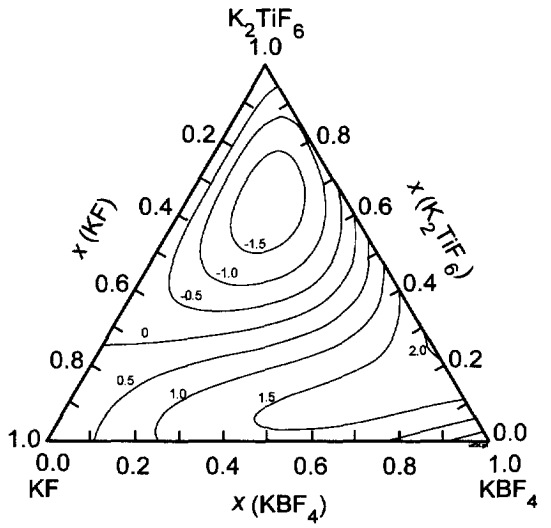

Fig. 24. Excess molar volume of the $KF–KBF_4–K_2TiF_6$ system at $T=1100$ K. Values are in $cm^3\ mol^{-1}$.

in Ref. [105]. The following equation was calculated for the molar volume at 1100 K

$$V/cm^3\ mol^{-1} = 30.57x_{KF} + 75.12x_{KBF_4} + 114.62x_{K_2TiF_6} + 5.41x_{KF}x_{KBF_4} + x_{KBF_4}x_{K_2TiF_6}(18.44 - 28.29x_{K_2TiF_6}) - 152.50x_{KF}x_{KBF_4}x_{K_2TiF_6} \quad (34)$$

with a standard deviation of fit $\sigma = 0.34\ cm^3\ mol^{-1}$. The excess molar volume of this system is shown in Fig. 24. The values of the constants calculated indicate, that from the volume properties point of view, the binary $KF–KBF_4$ system shows little deviations from ideal behaviour, while the $KF–K_2TiF_6$ system is ideal within experimental error. This is in harmony with the results reported in Refs. [83,96]. The ternary system also deviates only slightly from ideal behaviour. The maximum deviation at a temperature of 1100 K and a concentration of 25 mol% K_2TiF_6 attains 1.91 $cm^3\ mol^{-1}$, which is 2.2% of the molar volume of this melt. At higher concentrations of K_2TiF_6 (above 55 mol%) the excess molar volume attains small negative values.

For the partial molar volume of K_2TiF_6 in the binary $KBF_4–K_2TiF_6$ system at 1100 K

$$V(K_2TiF_6) = (114.62 - 28.29x^2_{KBF_4} + 43.36x^3_{KBF_4})\ cm^3\ mol^{-1} \quad (35)$$

and for $x(KBF_4)\rightarrow 1$, $V(K_2TiF_6) = 129.69\ cm^3\ mol^{-1}$. This value is higher than the molar volume of pure K_2TiF_6 (cf. the first term in Eq. (35)), indicating the formation of larger complex ions, e.g. TiF_7^{3-}.

The following equation was obtained for the partial molar volume of KBF_4

$$V(KBF_4) = (75.12 + 36.32x^2_{K_2TiF_6} - 43.36x^3_{K_2TiF_6})\ cm^3\ mol^{-1} \quad (36)$$

and for $x(K_2TiF_6) \rightarrow 1$, $V(KBF_4) = 68.08\ cm^3\ mol^{-1}$. This value is lower than the molar volume of pure KBF_4 (cf. the first term in Eq. (36)), due to decomposition of KBF_4 and escape of gaseous BF_3 from the melt, which was actually observed.

From these results the following possible chemical reactions may take place in the binary KBF_4–K_2TiF_6 system as well as in the ternary KF–KBF_4–K_2TiF_6 system

$$KBF_{4(l)} + K_2TiF_{6(l)} = K_3TiF_{7(l)} + BF_{3(g)} \quad (37)$$

$$K_3TiF_{7(l)} = K_2TiF_{6(l)} + KF_{(l)} \quad (38)$$

A Gibbs' energy of thermal dissociation of K_3TiF_7 (Eq. (38)), $\Delta_r G^0 = 0.963$ kJ mol^{-1}, was calculated from the equilibrium constant of this reaction given in Ref. [96]. For the formation Gibbs' energy of K_3TiF_7

$$\Delta G^0_{K_3TiF_7} = \Delta G^0_{KF} + \Delta G^0_{K_2TiF_6} - \Delta_r G^0(38) \quad (39)$$

For reaction Eq. (37) then

$$\Delta_r G^0(37) = \Delta G^0_{K_3TiF_7} + \Delta G^0_{BF_3} - \Delta G^0_{KBF_4} - \Delta G^0_{K_2TiF_6} \quad (40)$$

The Gibbs' energies of formation of BF_3, KBF_4 and KF were taken from Ref. [106] and $\Delta_r G^0(38)$ from Ref. [96]. From Eqs. (39) and (40) the Gibbs' energy of reaction Eq. (37), $\Delta_r G^0(37) = 10.71$ kJ mol^{-1} at $T = 1100$ K. The relatively low positive value of the reaction Gibbs' energy, as well as the escape of gaseous BF_3, indicate the probability of reaction Eq. (37) in the melt.

The excess molar volume of the ternary KF–KBF_4–K_2TiF_6 system is shown in Fig. 24. The maximum deviation from additivity is in the binary KBF_4–K_2TiF_6 system. Two different regions are present also in the ternary system: the region of volume expansion with a maximum at approx. 25 mol% K_2TiF_6 and 75 mol% KBF_4 and a region of volume contraction with a maximum at approx. 60 mol% K_2TiF_6 and 20 mol% KBF_4. We conclude that a chemical interaction according to Eq. (37) also plays a dominant role in the ternary system. However, the equilibrium of this reaction is shifted more to the left, because of the thermal dissociation of K_3TiF_7 and the presence of F^- ions, which suppress the formation of gaseous BF_3 in favour of BF_4^- complex ions.

The theoretical density course in the KBF_4–K_2TiF_6 system, calculated supposing reactions Eqs. (37) and (38) to take place, confirmed the above conclusions.

The viscosity of the KF–KBF_4–K_2TiF_6 melts [107] increases from KBF_4 through KF to K_2TiF_6. The viscosity of KBF_4 seems surprisingly low, however, there is a substantial overheating of the KBF_4 melt at 1100 K compared with that of KF.

The following equation has been calculated for the viscosity of this system at 1100 K

$$\eta/\text{mPa}\cdot\text{s} = 1.421^{x_{KF}} \times 0.638^{x_{KBF_4}} \times 4.247^{x_{K_2TiF_6}} - 0.489 x_{KF} x_{KBF_4} + 4.795 x_{KF} x_{K_2TiF_6}^4 + 4.385 x_{KBF_4} x_{K_2TiF_6}^4 + 0.079 x_{KF} x_{KBF_4}^5 x_{K_2TiF_6}^3 \quad (41)$$

with a standard deviation of fit $\sigma = 0.011$ mPa · s. The excess viscosity of the ternary $KF–KBF_4–K_2TiF_6$ system is shown in Fig. 25. In the binary $KF–KBF_4$ system negative deviations from ideal behaviour were observed. KBF_4 tends to share BF_4^- tetrahedra forming relatively weak B–F–B bridges. In introducing F^- ions into the melt by addition of KF, the B–F–B bridges break, leading to the lowering of viscosity.

In the binary $KF–K_2TiF_6$ system the additive compound K_3TiF_7 is formed, which increases the viscosity of the melt. Therefore the excess viscosity in this system is positive.

As in the density measurements [105], the positive deviation from ideal behaviour in the binary $KBF_4–K_2TiF_6$ system is caused by the formation of more voluminous TiF_7^{3-} anions.

From the statistically important ternary interaction described by the last term in Eq. (41) the chemical reaction Eq. (37) together with the thermal dissociation of K_3TiF_7 also take place in the ternary $KF–KBF_4–K_2TiF_6$ system.

The results of the viscosity measurement thus confirmed the conclusions drawn from the phase diagram and density measurements.

4.2.4. *Subsystem KCL–KBF$_4$–K$_2$TiF$_6$*

The phase diagram of the ternary $KCl–KBF_4–K_2TiF_6$ system was determined in Ref. [108] using the thermal analysis method. To obtain a thermodynamically consistent phase diagram a subsequent coupled analysis of the thermodynamic and phase

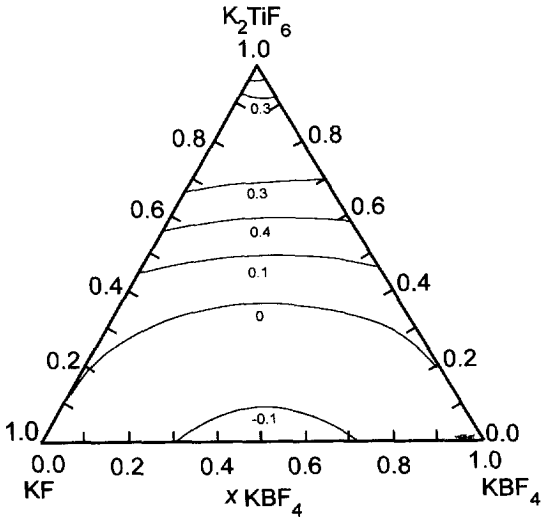

Fig. 25. Excess viscosity of the $KF–KBF_4–K_2TiF_6$ system. Values are in mPa · s.

diagram data was performed. Four crystallisation fields are present in the phase diagram of the KCl–KBF_4–K_2TiF_6 system (Fig. 26) corresponding to the primary crystallisation of KCl, KBF_4, K_2TiF_6 and the intermediate compound K_3TiF_6Cl. The calculated co-ordinates of the two ternary eutectic points are:

e_1: 24.1 mol% KCl, 62.1 mol% KBF_4, 13.8 mol% K_2TiF_6, $t_{e1}=447.1$ °C;

e_2: 6.5 mol% KCl, 62.5 mol% KBF_4, 31.0 mol% K_2TiF_6, $t_{e2}=414.5$ °C.

The probable maximum inaccuracy in the calculated ternary phase diagram is ±17.1 °C.

The following equation was obtained for the molar excess Gibbs' energy of mixing

$$\Delta G^E/\text{J mol}^{-1} = 1745x_{KCl}x_{KBF_4} - x_{KCl}x_{K_2TiF_6}(6906 + 10055x_{K_2TiF_6}) - x_{KBF_4}x_{K_2TiF_6}(6092 - 14202x^2_{K_2TiF_6}) - 36401x^2_{KCl}x_{KBF_4}x_{K_2TiF_6} \quad (42)$$

The first term represents the molar excess Gibbs' energy of mixing in the binary KCl–KBF_4 system, the second in the binary KCl–K_2TiF_6 system and the third in the binary KBF_4–K_2TiF_6 system. The last term represents the interaction contribution in the ternary system. The molar excess Gibbs' energy of mixing in the ternary KCl–KBF_4–K_2TiF_6 system is shown in Fig. 27.

The phase diagram of the boundary KCl–KBF_4 system (Fig. 28) shows a symmetrical concentration dependence of the molar excess Gibbs' energy of mixing indicating that simple regular solutions are formed. The calculated concentration co-ordinates of the eutectic point 72.9 mol% KBF_4 and 27.1 mol% KCl are relatively

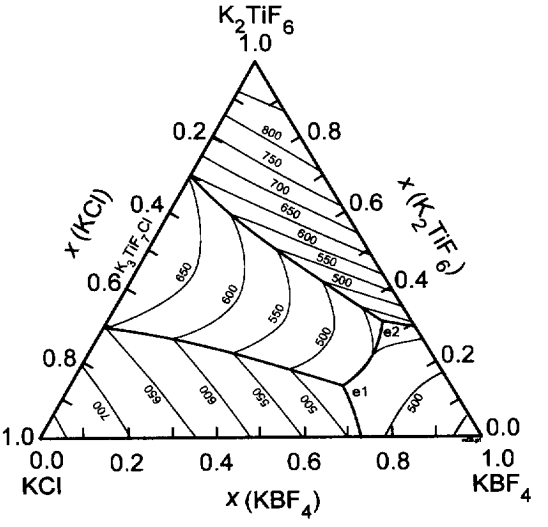

Fig. 26. Phase diagram of the KCl–KBF_4–K_2TiF_6 system.

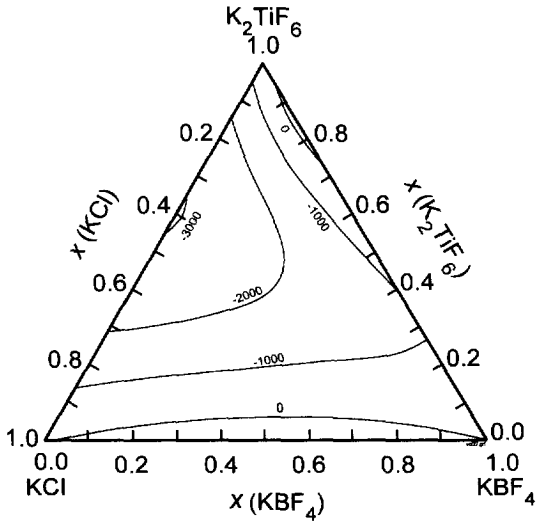

Fig. 27. Excess Gibbs' energy of mixing of the KCl–KBF_4–K_2TiF_6 system. Values are in J mol^{-1}.

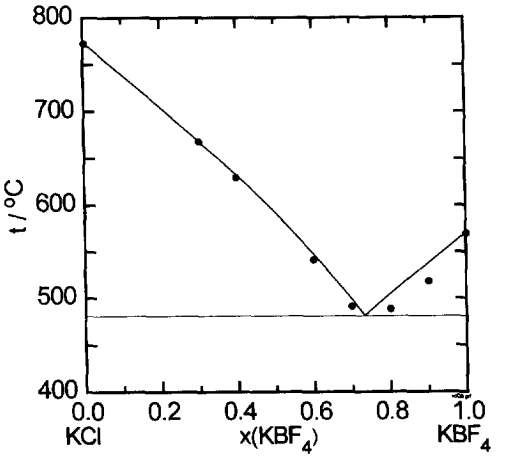

Fig. 28. Phase diagram of the KCl–KBF_4 system.

close to those given in Ref. [77], while the calculated eutectic temperature, 481.7 °C, is substantially higher.

The phase diagram of the boundary KCl–K_2TiF_6 system (Fig. 29) is described by a second order polynomial for the molar excess Gibbs' energy of mixing. The co-ordinates of both eutectic points (e_1: 29.7 mol% K_2TiF_6, 654.0 °C; e_2: 70.0 mol% K_2TiF_6, 642.3 °C) differ from those given in Ref. [99], probably due to appreciable inaccuracy in the determination of the liquidus temperature.

Similar results to those in Ref. [103] were also obtained for the boundary

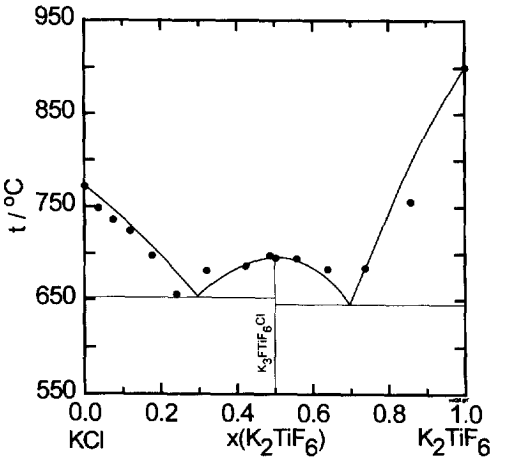

Fig. 29. Phase diagram of the KCl–K_2TiF_6 system.

KBF_4–K_2TiF_6 system, where a third order polynomial for the molar excess Gibbs' energy of mixing and close co-ordinates of the eutectic point were found. Again the significant inflex course of the K_2TiF_6 liquidus curve is most probably due to decomposition of KBF_4 and escape of gaseous BF_3.

The density of the KCl–KBF_4–K_2TiF_6 melts has been measured [109] using the Archimedean method. The molar volume, the partial molar volume and the excess molar volume of the melts were calculated on the basis of density data and possible chemical interactions were considered.

The following equation was obtained for the molar volume of the ternary system after considering the linear temperature dependence of the molar volumes of the pure components as well as those of the binary and ternary interactions

$$\begin{aligned} V/\mathrm{cm^3\ mol^{-1}} = {} & x_{\mathrm{KCl}}(34.450 + 1.879 \times 10^{-2} T/\mathrm{K}) \\ & + x_{\mathrm{KBF_4}}(50.760 + 2.982 \times 10^{-2} T/\mathrm{K}) \\ & + x_{\mathrm{K_2TiF_6}}(86.149 + 3.383 \times 10^{-2} T/\mathrm{K}) \\ & + 3.985 x_{\mathrm{KCl}} x_{\mathrm{KBF_4}}^2 + x_{\mathrm{KCl}} x_{\mathrm{K_2TiF_6}} \\ & \times (8.883 x_{\mathrm{K_2TiF_6}} - 7.624 \times 10^{-3} T/\mathrm{K}) \\ & - x_{\mathrm{KBF_4}} x_{\mathrm{K_2TiF_6}} (14.776 - 1.447 \times 10^{-2} T/\mathrm{K}) \\ & - 88.661 x_{\mathrm{KCl}} x_{\mathrm{KBF_4}} x_{\mathrm{K_2TiF_6}}^2 \end{aligned} \quad (43)$$

The standard deviation of Eq. (43) is $\sigma = 0.343\ \mathrm{cm^3\ mol^{-1}}$.

From comparison of the experimentally determined values of the molar volumes of the ternary KCl–KBF_4–K_2TiF_6 system with those calculated according to Eq. (43) it follows that there is a significant ternary interaction. The standard deviation of approximation agrees well with the experimental error.

The calculated values of the excess molar volume for the binary $KCl–KBF_4$ system (Fig. 30) differ only slightly from additive behaviour, in agreement with the results given in Ref. [83]. In the $KBF_4–K_2TiF_6$ and $KCl–K_2TiF_6$ systems deviations from ideal behaviour are larger. In the former system the deviations are positive, while in the latter one they are negative.

As in the ternary $KF–KBF_4–K_2TiF_6$ system [105], two different regions are present in the ternary $KCl–KBF_4–K_2TiF_6$ system (Fig. 31): A region of volume

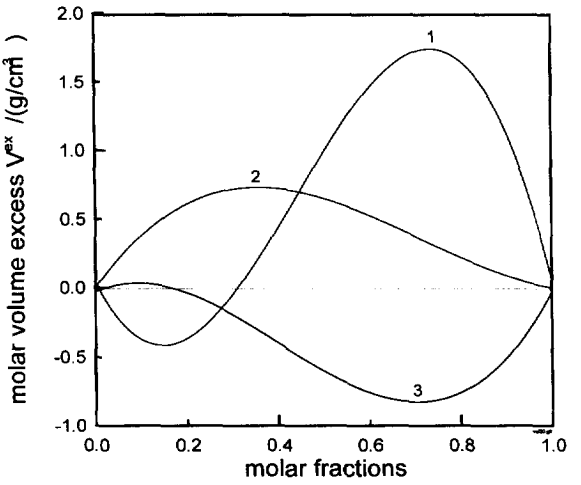

Fig. 30. Excess molar volumes of the boundary binary systems at $T=1100$ K. (1) $KCl–KBF_4$; (2) $KCl–K_2TiF_6$; (3) $KBF_4–K_2TiF_6$.

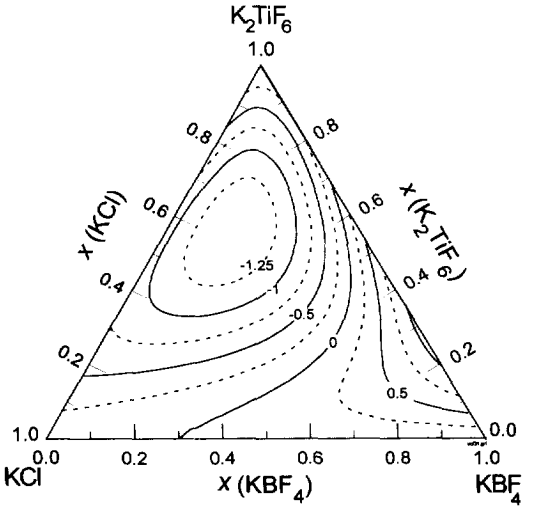

Fig. 31. Excess molar volume of the $KCl–KBF_4–K_2TiF_6$ system at $T=1100$ K. Values are in $cm^3\ mol^{-1}$.

expansion with the maximum in the binary KBF_4–K_2TiF_6 system at approx. 25 mol% K_2TiF_6 and 75 mol% KBF_4 and a region of volume contraction with the maximum at approx. 60 mol% K_2TiF_6, 20 mol% KCl and 20 mol% KBF_4. On this basis, as well as from the last coefficient in Eq. (43), a ternary interaction exists in melts of the KCl–KBF_4–K_2TiF_6 system.

In the molten KBF_4–K_2TiF_6 system the chemical reactions Eqs. (37) and (38), it is suggested [105] take place. The additive compound K_3TiF_6Cl, formed in the binary KCl–K_2TiF_6 system, also dissociates thermally according to

$$K_3TiF_6Cl_{(l)} = K_2TiF_{6(l)} + KCl_{(l)} \tag{44}$$

$$\Delta_r G^0_{1100\ K} = 0.587\ \text{kJ mol}^{-1}$$

The Gibbs' energy of reaction Eq. (44) was calculated from the equilibrium constant of this reaction in Ref. [96].

In the ternary KCl–KBF_4–K_2TiF_6 system the following chemical reaction is possible

$$KCl(l) + 2K_2TiF_6(l) + KBF_4(l) = K_3TiF_7(l) + K_3TiF_6Cl(l) + BF_3(g)\ \Delta_r G^0_{1100\ K} = 12.05\ \text{kJ mol}^{-1} \tag{45}$$

The resulting additive compounds dissociate thermally according to reactions Eqs. (38) and (44). The Gibbs' energy of reaction Eq. (45) was calculated on the basis of the Gibbs' energies of reactions Eqs. (38) and (44), as well as of the Gibbs' energies of formation of KCl, KBF_4 and BF_3 given in Ref. [106]. The relatively low positive value of the reaction Gibbs' energy and the observed slow escape of gaseous BF_3 indicate that reaction Eq. (45) probably takes place in the ternary melts.

The excess viscosity in the ternary KCl–KBF_4–K_2TiF_6 system was measured in Ref. [110] and information on the interactions of components and on the probable structure of the melts was obtained.

The following equation was obtained for the viscosity of the KCl–KBF_4–K_2TiF_6 system at $T = 1100$ K

$$\eta/\text{mPa}\cdot\text{s} = 0.960^{x_{KCl}} \times 0.631^{x_{KBF_4}} \times 4.342^{x_{K_2TiF_6}} - 0.644 x_{KCl} x^2_{KBF_4} - 2.427 x_{KCl} x_{K_2TiF_6} - 2.549 x_{KBF_4} x_{K_2TiF_6} - 63.784 x_{KCl} x^2_{KBF_4} x^2_{K_2TiF_6} \tag{46}$$

with a standard deviation $\sigma = 0.033$ mPa · s. The excess viscosity at 1100 K based on Eq. (46) is shown in Fig. 32. There are two different regions in the ternary system. The first region with low K_2TiF_6 concentration shows negative deviations in the viscosity, while in the second region with higher K_2TiF_6 concentration, positive excess viscosity is observed. The excess viscosity course in the binary systems is shown in Fig. 33. Since there is a common cation, the observed deviations may be ascribed to the mutual interactions of anions.

In the binary KCl–KBF_4 system exchange of fluorine atoms in the BF_4^- tetrahedra by chlorine takes place in the melt with the presence of $[BF_{4-n}Cl_n]^-$. The less stable

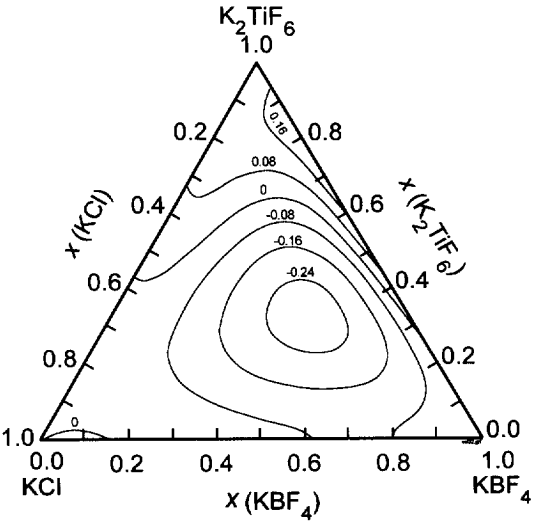

Fig. 32. Excess viscosity of the $KCl–KBF_4–K_2TiF_6$ system at $T=1100$ K. Values are in mPa·s.

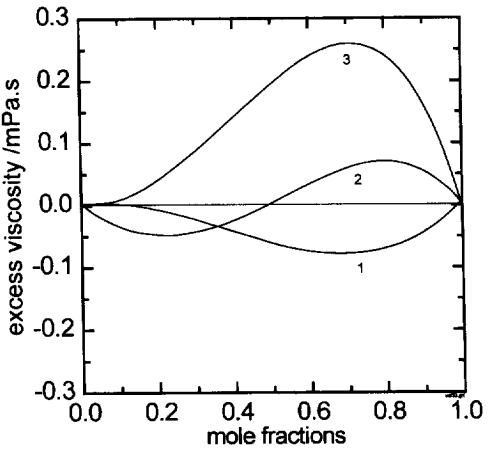

Fig. 33. Excess viscosity of the boundary binary system at $T=1100$ K. (1) $KCl–KBF_4$; (2) $KCl–K_2TiF_6$; (3) $KBF_4–K_2TiF_6$.

B–Cl–B bridges and the lower concentration of the B–F–B bridges most probably cause the negative deviations in the viscosity course.

In the binary $KCl–K_2TiF_6$ system the intermediate compound K_3TiF_6Cl is formed. However, the stability of this compound is low and its presence affects the viscosity course positively only at high concentrations of K_2TiF_6.

In the binary $KBF_4–K_2TiF_6$ system the reaction Eq. (37) takes place. In spite of the extended thermal dissociation of K_3TiF_7, the Gibbs' energy of reaction Eq. (37)

has a relatively low positive value, leading to the significant presence of K_3TiF_7 in the melt and to a positive deviation in the viscosity course.

From the statistically important ternary interaction (the last term in Eq. (46)) it follows that reaction Eq. (45) takes place in the ternary KCl–KBF_4–K_2TiF_6 system.

From thermodynamic and physico-chemical analysis of the KF–KCl–KBF_4–K_2TiF_6 melts it follows that their most characteristic feature is the formation of the thermodynamically less stable TiF_7^{3-} and TiF_6Cl^{3-} anions with lower co-ordination symmetry. The presence of these anions in the melt most probably facilitates the electroreduction of titanium and thus the formation of titanium diboride on the cathode.

5. Deposition of aluminium

Aluminium is generally produced by electrolytic reduction of aluminium oxide dissolved in molten cryolite. A comprehensive review on the theory and knowledge of aluminium electrolysis to 1980 was published by Grjotheim et al. [111], and later by Grjotheim and Welch [112], and Grjotheim and Kvande [113]. A recent review of basic knowledge was presented by Haupin [114].

Although the mechanism of the electrolytic process is not yet fully understood, there is relatively detailed insight into the structure of the electrolyte. It is generally agreed that molten cryolite dissociates completely into sodium (Na^+) cations and hexafluoroaluminate (AlF_6^{3-}) anions. According to the classic idea represented by Grotheim et al. [111] the AlF_6^{3-} anions partially dissociate according to the scheme

$$AlF_6^{3-} = AlF_4^- + 2F^- \tag{47}$$

On the other hand, recent investigations based on Raman spectroscopic measurements [115–117] suggest the two-step dissociation of the AlF_6^{3-} anions according to the schemes

$$AlF_6^{3-} = AlF_5^{2-} + F^- \tag{48}$$

$$AlF_5^{2-} = AlF_4^- + F^- \tag{49}$$

The final anionic composition of the NaF–AlF_3 melts depends on the cryolite ratio ($CR = n(NaF)/n(AlF_3)$) and the temperature. Fluorides are sometimes added to the electrolyte to lower the temperature of primary crystallisation and to increase the efficiency of the electrolysis. The most common additive is aluminium fluoride, the content of which varies in the range 3–14 mass% AlF_3 in excess of the Na_3AlF_6 composition.

5.1. Structure of cryolite–alumina melts

During the approximately half century of investigation of the structure of the cryolite–alumina melts there have been numerous suggestions on the nature of the

possible oxygen-containing species present in the melt [111]. The older works [118–130] assumed the presence of different aluminate and oxyfluoroaluminate anions such as AlO_2^-, AlO_3^{3-}, $AlOF_3^{2-}$ and $AlOF_5^{4-}$. However, the nature of the dominating species at different alumina concentrations in the melt and at different cryolite ratios still remains the most important task in aluminium electrolyte chemistry.

In the last two decades it was generally accepted that complex oxyfluoroaluminate anions are the most probable species formed. Dewing [131] suggested that alumina dissolves predominantly with formation of $AlOF_x^{1-x}$ anions, while Ratkje and Forland [132,133] on the basis of cryoscopic measurements indicated the following equilibrium reaction

$$Al_2OF_x^{4-x} = AlOF_y^{1-y} + AlF_{x-y}^{(3-x+y)} \tag{50}$$

Probable values for x are 6 or 8, while y may be 2, indicating that $AlF_{x-y}^{(3-x+y)}$ is then AlF_6^{3-} or AlF_4^-, the most important anions in oxide-free cryolite melts.

More recent investigations, based mainly on Raman spectroscopic measurements [115,116] indicate that anions with bridging Al–O–Al bonds are really present, most probably having the following structure

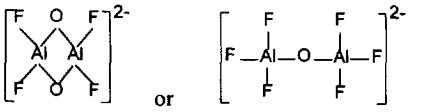

(51)

These species originate in the melt by reaction of AlF_6^{3-} with dissolved alumina.

New insight into the character of the oxyfluoroaluminate species was brought by Gilbert et al. [117,134] on the basis of Raman spectroscopy. The Raman spectra excluded the presence of species with non-bridging Al–O bonds and only those having bridging Al–O–Al bond, corresponding to $Al_2OF_x^{4-x}$ complexes, are considered.

Sterten [135] developed an ionic model of the cryolite melts saturated with alumina on the basis of the experimentally determined activities for NaF and AlF_3. He found out that the $Al_2OF_x^{4-x}$ and $Al_2O_2F_x^{2-x}$ species are most probably present in these cryolite–alumina melts. The species $AlOF_x^{1-x}$ were found to be of minor importance. He claimed that in very basic melts ($CR > 5$) $Al_2O_2F_4^{2-}$ and $Al_2O_2F_6^{4-}$ complexes are dominating, while in acidic melts ($CR < 3$) the complexes $Al_2OF_6^{2-}$ and $Al_2O_2F_4^{2-}$ are the most abundant.

Julsrud [136] proposed a thermodynamic model for cryolite–alumina melts based on cryoscopic and calorimetric measurements and considered the $Al_2OF_6^{2-}$, $Al_2OF_8^{4-}$, $Al_2OF_{10}^{6-}$, $Al_2O_2F_4^{2-}$ and $Al_2O_2F_6^{4-}$ species to be present in these melts. Kvande [137,138] also suggested that $Al_2OF_8^{4-}$ is the most abundant species in the low alumina cryolite melts.

The solubility of alumina in $NaF–AlF_3$ melts attains a maximum at the composition of cryolite [111,138]. Therefore, it is reasonable to assume that alumina, when dissolving in cryolite-based melts, reacts predominantly with AlF_6^{3-} anions according

to the following reaction schemes

$$Al_2O_3 + 4AlF_6^{3-} = 3Al_2OF_6^{2-} + 6F^- \quad (52)$$

$$Al_2O_3 + 4AlF_6^{3-} = 3Al_2OF_8^{4-} \quad (53)$$

$$Al_2O_3 + AlF_6^{3-} = 3/2Al_2O_2F_4^{2-} \quad (54)$$

Reactions of alumina with F^- ions are less probable, since the alumina solubility in pure molten NaF is very low.

An alternative reaction sequence may first be the dissociation of Al_2O_3 according to the schemes

$$Al_2O_3 \rightarrow 2AlO^+ + O^{2-} \quad (55)$$

$$Al_2O_3 \rightarrow Al_2O^{4+} + 2O^{2-} \quad (56)$$

and the subsequent reaction of the dissociation products with AlF_6^{3-} anions with formation of the three main oxygen-containing species, $Al_2OF_6^{2-}$, $Al_2OF_8^{4-}$ and $Al_2O_2F_4^{2-}$

$$2AlO^+ + O^{2-} + 4AlF_6^{3-} \rightarrow 3Al_2OF_6^{2-} + 6F^- \quad (57)$$

$$2AlO^+ + O^{2-} + 4AlF_6^{3-} \rightarrow 3Al_2OF_8^{4-} \quad (58)$$

$$2AlO^+ + O^{2-} + AlF_6^{3-} \rightarrow 3/2Al_2O_2F_4^{2-} \quad (59)$$

The arrows indicate that the reactions are shifted completely to the right. The second dissociation scheme of alumina seems to be of less importance, since it is not expected that Al_2O^{4+} ions would react with AlF_6^{3-} ions with formation of species with three aluminium atoms.

The above picture of the cryolite–alumina melts was also recently confirmed by very accurate Raman spectra measurements and vapour pressure carried out by Gilbert et al. [134]. Similar reactions accompanying the dissolution of alumina were suggested, however, the AlF_5^{2-} anion was considered to be the most abundant species and thus as a reactant needed further F^- ions to use in the above reaction schemes.

The very recent investigation of Danek and Østvold [139], based on direct oxygen determination in cryolite–alumina melts with dependence on the cryolite ratio and alumina content, confirmed the predominant presence of $Al_2OF_6^{2-}$, resp. $Al_2OF_8^{4-}$, species in the low alumina-containing melts, while at higher alumina content all three species, $Al_2OF_6^{2-}$, $Al_2OF_8^{4-}$ and $Al_2O_2F_4^{2-}$ are present, regardless of cryolite ratio.

5.2. Electrode reactions

The mechanism of the electrode reactions with regard to the structure of cryolite–alumina melts is probably at present one of the most widely investigated subjects in aluminium electrochemistry. Although neither the anode nor the cathode reaction is fully understood, enough is known to form a reasonably consistent picture.

5.2.1. Anode reactions

The anode reaction may be written in the simple form

$$C + 2O^{2-} \rightarrow CO_2 + 4e^- \quad (60)$$

but free oxide ions do not exist in the electrolyte. It is generally accepted that the oxygen is transported to the anode in the form of Al–O–F complexes. The equations for possible anode reactions involving the three main species are as follows

$$2Al_2OF_6^{2-} + C + 4F^- = CO_2 + 4e^- + 4AlF_4^- \quad (61)$$

$$2Al_2OF_8^{4-} + C = CO_2 + 4e^- + 4AlF_4^- \quad (62)$$

$$Al_2O_2F_4^{2-} + C + 4F^- = CO_2 + 4e^- + 2AlF_4^- \quad (63)$$

All these reactions involve the formation of AlF_4^- ions thus explaining why the electrolyte becomes more acidic close to the anode during electrolysis.

Sterten [135] calculated from bond energies that the first oxygen atom can be removed from $Al_2O_2F_4^{2-}$ much easier than the second or the one oxygen from $Al_2OF_6^{2-}$. This suggests that the anode reaction is

$$2Al_2O_2F_4^{2-} + C \rightarrow CO_2 + Al_2OF_4 + 4e^- \quad (64)$$

The equilibrium between $Al_2O_2F_4^{2-}$ and $Al_2OF_6^{2-}$ can be restored by reaction

$$Al_2OF_6^{2-} + Al_2OF_4 \Leftrightarrow Al_2O_2F_4^{2-} + 2AlF_3 \quad (65)$$

with AlF_3 reacting subsequently with F^- to form AlF_4^- ions. However, the presence of any neutral molecules such as Al_2OF_4 is not probable in these ionic melts.

5.2.2. Cathode reactions

Since Al^{3+} cations cannot be present in the electrolyte, aluminium is deposited from anionic complexes only. The primary deposition of sodium does not take place, since the voltage required for aluminium deposition is about 0.22 V lower than that required for deposition of sodium. The main cathode reaction is often written in the form

$$AlF_4^- + 3e^- \rightarrow Al + 4F^- \quad (66)$$

However, recent work by Thonstad [114,140] indicated that aluminium is discharged from oxyfluoroaluminate ions by a three-step process with charge transfer taking place in two steps

$$Al_2OF_6^{2-} \Leftrightarrow Al_2OF_4 + 2F^- \quad (67)$$

$$Al_2OF_4 + 2e^- \Leftrightarrow AlF_{2(ads)}^- + AlOF_2^- \quad (68)$$

$$AlF_{2(ads)}^- + e^- \rightarrow Al + 2F^- \quad (69)$$

The notation (ads) means that these species are adsorbed on the cathode surface. Na^+ carries the current and is transported to the cathode interface. $Al_2OF_6^{2-}$ diffuses

to the interface and 2 Na^+ accompany it to maintain charge neutrality. The stepwise discharge of one $Al_2OF_6^{2-}$ ion produces one atom of liquid aluminium, one $AlOF_2^-$ ion and 4 F^- ions. The 4 F^- and one $AlOF_2^-$ ions set free are just sufficient to neutralise the space charge of the 5 Na^+ cations, three transported by the current and two that accompanied $Al_2OF_6^{2-}$. The originating $AlOF_2^-$ ion can react with AlF_4^- to produce the next $Al_2OF_6^{2-}$ ions. Both cathode mechanisms result at the cathode interface in a high concentration of NaF which can actually be determined.

In both anodic and cathodic processes the less symmetrical oxyfluoroaluminate complexes are involved. Thus, the lower symmetry of these anions is most probably responsible for the easy deposition of aluminium. This may also be supported by many unsuccessful attempts of one of the founders of this process, P.L.T. Héroult, to produce aluminium from pure cryolite [111]. The favourable effect of alumina was confirmed recently by Makyta et al. [22] using voltammetric measurements in the Na_3AlF_6–Al_2O_3 system. Fig. 34 shows the cathodic part of the voltammetric curves recorded in pure cryolite (curve 1) and in the melt containing 2 mol% of Al_2O_3 (curve 2). Comparison of both curves shown in the figure confirms that the introduction of oxygen-containing species to the molten cryolite favourably influences the deposition of aluminium. The electrodeposition potential of aluminium is shifted to more positive values and the peak current, which represents the amount of electrochemical active aluminium species in the melt, increases.

However, it is very difficult to prepare oxygen-free pure cryolite. Even the Greenland hand-picked natural cryolite or synthetic cryolite prepared from sublimated AlF_3 may contain a small amount of alumina. Contamination of cryolite by moisture may also occur during the preparation of samples despite careful treatment in a glove box. Thus, the problem of oxygen-free cryolite preparation and the verification of the possibility to deposit aluminium from oxygen-free cryolite may be the objective of a further investigation.

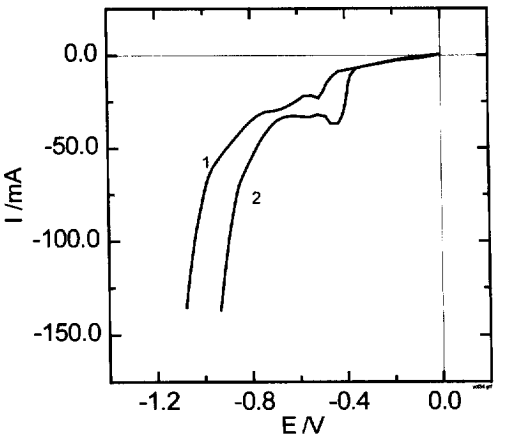

Fig. 34. Voltametric curves recorded in the Na_3AlF_6–Al_2O_3 system using molybdenum as a working electrode, polarisation rate 0.5 V s^{-1}. (1) Na_3AlF_6; (2) Na_3AlF_6 + 2 mol% Al_2O_3.

The crucial importance of the presence of oxyfluoroaluminate species is also indicated by the so-called anode effect, which takes place during electrolysis when the alumina concentration in the electrolyte is nearly depleted. As alumina is depleted, the anode overvoltage increases causing reduced wetting of the anode and the formation of fluorocarbon compounds, e.g. CF_4, which form a gas film on the anode. Since the three main species, $Al_2OF_6^{2-}$, $Al_2OF_8^{4-}$ and $Al_2O_2F_4^{2-}$, are in chemical equilibrium the anode effect cannot be caused by the consumption of only one of them, because the chemical equilibrium would be shifted in order to counteract the change. It seems more reasonable to assume that the total amount of these species is important [138]. This means that the anode effect occurs because there is a lack of Al–O–F species in the melt. On the other hand, it is also possible that equilibrium conditions do not exist during electrolysis, and that slow mass-transfer will cause a concentration gradient of the oxygen-containing species near the anode. Thus, the anode effect may occur because the concentration of these species close to the anode surface becomes zero.

6. Conclusions

On the basis of the current review, ionic structure and especially the local structure of the electroactive species, plays a key role in the mechanism of the electrodeposition of metals from molten salts. It is clearly demonstrated in the examples presented above that the creation of species containing electrodeposited metal and exhibiting lowered symmetry of the co-ordination sphere enables metal deposition (molybdenum, aluminium) or enhances the rate of its deposition (titanium).

Molybdenum is electrodeposited from B_2O_3–K_2MoO_4 and KF–B_2O_3–K_2MoO_4 electrolytes most probably due to the presence of complex heteropolyanions in the melt. The electrodeposition of titanium from K_2TiF_6 is enhanced by the formation of TiF_7^{3-} or TiF_6Cl^{3-} anions which are present in the molten KF–K_2TiF_6 and KCl–K_2TiF_6 melts, respectively. The formation of complex aluminium oxyfluoroaluminate species is responsible for electrodeposition of aluminium from cryolite–alumina melts.

Acknowledgements

The present work was financially supported by the Scientific Grant Agency of the Ministry of Education of the Slovak Republic and the Slovak Academy of Sciences under the No's. 2/1164/96, 2/2067/96 and 2/2068/96.

References

[1] K. Koyama, Y. Hashimoto, S. Omori, K. Terawaki, J. Less-Common Met. 132 (1987) 57.
[2] M. Makyta, P. Zatko, P. Bezdicka, Chem. Pap. 47 (1993) 28.

[3] P. Zatko, M. Makyta, J. Sýkorová, A. Silný, Chem. Pap. 48 (1994) 10.
[4] W. Stortenbeker, Z. Physik. Chem. 10 (1892) 183.
[5] S. Senderoff, A. Brenner, J. Electrochem. Soc. 101 (1954) 16.
[6] A.N. Baraboshkin, N.A. Saltykova, M.I. Talanova, Z.S. Martemyanova, Elektrokhim. 6 (1970) 1552.
[7] A.N. Baraboshkin, N.A. Saltykova, A.M. Molchanov, M.I. Talanova, Z.S. Martemyanova, Elektrokhim. 8 (1972) 833.
[8] A.N. Baraboshkin, N.A. Saltykova, M.I. Talanova, A.M. Molchanov, Trudy Inst. Elektrokhim. UFAN, USSR 20 (1973) 65.
[9] A.K. Suri, C.K. Gupta, J. Less-Common Met. 31 (1973) 389.
[10] G.W. Mellors, S. Senderoff, US Patent 3 444 058, May 13, 1969.
[11] F.X. McCawley, Ch. Wyche, D. Schlein, J. Electrochem. Soc. 116 (1969) 1028.
[12] B.N. Popov, H.A. Laitinen, J. Electrochem. Soc. 120 (1973) 1346.
[13] V.I. Shapoval, V.F. Makogon, Elektrokhim. 12 (1976) 1723.
[14] K. Koyama, Y. Hashimoto, S. Omori, K. Teravaki, Trans. Jpn. Inst. Met. 25 (1984) 265.
[15] K. Koyama, Y. Hashimoto, S. Omori, K. Teravaki, Trans. Jpn. Inst. Met. 25 (1984) 804.
[16] K. Teravaki, Trans. Jpn. Inst. Met. 26 (1985) 198.
[17] A.N. Baraboshkin, A.F. Shunailov, V.A. Martinov, Trudy Inst. Elektrokhim., Akad. Nauk SSSR 15 (1970) 44.
[18] S. Senderoff, G.W. Mellors, J. Electrochem. Soc. 114 (1967) 556.
[19] S. Senderoff, A. Brenner, J. Electrochem. Soc. 101 (1954) 31.
[20] V.I. Shapoval, A.Sh. Avaliyani, N.A. Gasviyani, Elektrokhim. 12 (1976) 1097.
[21] Li Guoxun, Fan Defang, Trans. Non-Ferrous Met. Soc. China 1 (1991) 39.
[22] M. Makyta, P. Zatko, V. Danek, Influence of the melt structure on the deposition of molybdenum, titanium and aluminium, in: Proc. IX. Int. Symp. Molten Salts, San Francisco, May 1994.
[23] M. Makyta, T. Utigard, P. Zatko, A. Silný, M. Chrenková, Chem. Pap. 51 (1997) 202; M. Makyta, T. Utigard, P. Zatko, A. Silný, V. Danek, Chem. Pap. 51 (1997) 208.
[24] M. Makyta, Chem. Pap. 47 (1993) 306.
[25] H. Rawson, Inorganic Glass-Forming Systems, Academic Press, London, 1967, pp. 207–208.
[26] V. Danek, M. Chrenková, Chem. Pap. 47 (1993) 339.
[27] P. Delahay, T. Berzins, J. Am. Chem. Soc. 75 (1953) 2486; 75 (1953) 4205.
[28] A. Silný, P. Zatko, M. Makyta, J. Sýkorová, in: C.A.C. Sequeira, G.S. Picard (Eds.), Molten Salts Forum, vols. 1–2, Trans Tech Publications, Zürich, 1993, pp. 155–160.
[29] P. Zatko, Voltametric measurements in the system $KF–K_2MoO_4–SiO_2$, in: Proc. 49 Chemical Soc. Meeting, Bratislava, September 1995, p. 280.
[30] I. Koštenská, M. Malinovský, Chem. Zvesti 36 (1982) 159.
[31] M. Chrenková, V. Danek, A. Silný, Thermochim. Acta 231 (1994) 79.
[32] O. Schmitz-Dumont, A. Weeg, Z. Anorg. Chem. 265 (1951) 1673.
[33] Z.A. Mateiko, G.A. Bukhalova, Zh. Obshch. Khim. 25 (1955) 1673.
[34] S. Julsrud, O.J. Kleppa, Acta Chem. Scand. A35 (1981) 669.
[35] O. Patarák, Z. Jantáková, V. Danek, Chem. Pap. 47 (1993) 342.
[36] O. Patarák, PhD Thesis, Institute of Inorganic Chemistry, Slovak Academy of Sciences, Bratislava, 1995.
[37] L. Kosa, I. Nerád, O. Patarák, I. Proks, J. Strecko, K. Adamkovicová, Themochim. Acta 244 (1994) 69.
[38] M. Chrenková, V. Danek, Chem. Pap. 46 (1992) 222.
[39] M. Chrenková, V. Danek, A. Silný, Z. Anorg. Allg. Chem. 620 (1994) 385.
[40] M. Malinovský, I. Roušar, et al., Theoretical Fundamentals of Inorganic Technological Processes I, Alfa Publishers, Prague, 1987, p. 67.
[41] A. Silný, V. Danek, M. Chrenková, Ber. Bunsenges. Phys. Chem. 99 (1995) 74.
[42] P. Znášik, M. Jamnický, J. Non-Cryst. Solids 146 (1992) 74.
[43] M. Jamnický, P. Znášik, D. Tunega, M.D. Ingram, J. Non-Cryst. Solids 185 (1995) 151.
[44] K. Billehaug, H.A. Oye, Aluminium 56 (1980) 642.
[45] L. Andrieux, Ann. Chim. 12 (1929) 423.

[46] P.N. Nies, C.A. Morgan, G.P. Jones, Br. Patent 861 743 (1961).
[47] A.K. Ganesan, Indian Chem. J. (1972) 37.
[48] J.N. Gomes, K. Uchida, US Patent 3 775 271 (1973).
[49] D. Schlain, F.X. McCawley, G.R. Smith, US Bureau of Mines, Rep. Invest. (1976) 8146.
[50] D. Schlain, F.X. McCawley, Ch. Wyche, J. Electrochem. Soc. 116 (1969) 1227.
[51] F.X. McCawley, Ch. Wyche, D. Schlain, US Patent 3 697 390 (1972).
[52] V. Danek, K. Matiašovský, Koroze a Ochrana Materiálu 17 (1973) 89.
[53] F.X. McCawley, Ch. Wyche, D. Schlain, US Patent 3 827 954 (1974).
[54] D.R. Flin, F.X. McCawley, G.R. Smith, P.B. Needham, US Bureau of Mines, Rep. Invest. (1979) 8332.
[55] A. Bogacz, P. Los, W. Szklarski, J. Josiak, Rudy Metale 28 (1983) 134.
[56] M. Makyta, T. Utigard, Light Metals 1993, Warrendale, PA:TMS, 1993, p. 1137.
[57] R. Baboian, D.L. Hill, R.A. Bailey, Can. J. Chem. 43 (1965) 197.
[58] C. Guang-Sen, M. Okido, T. Oki, J. Appl. Electrochem. 17 (1987) 849; ibid 18 (1988) 80; Electrochem. Acta 32 (1987) 1637.
[59] E. Chassaing, F. Basile, G. Lorthioir, J. Less-Common Met. 58 (1979) 153.
[60] E. Chassaing, F. Basile, G. Lorthioir, J. Appl. Electrochem. 11 (1981) 187.
[61] D. Ferry, E. Noyon, G. Picard, J. Less-Common Met. 97 (1984) 331.
[62] D. Ferry, G. Picard, B. Tremillon, Trans. Inst. Min. Metall. Sect. C97 (1988) 21.
[63] C.A.C. Sequeira, J. Electroanal. Chem. 239 (1988) 203.
[64] J. De Lepinay, P. Paillere, Electrochim. Acta 29 (1984) 1243.
[65] J. De Lepinay, J. Bouteillon, S. Traore, D. Renaud, M. Barbier, J. Appl. Electrochem. 17 (1987) 294.
[66] K. Matiašovský, K. Grjotheim, M. Makyta, Metall. 42 (1988) 1192.
[67] M. Makyta, M. Matiašovský, V.I. Taranenko, Electrochim. Acta 34 (1989) 861.
[68] V.I. Taranenko, I.V. Zarutskii, V.I. Shapoval, M. Makyta, K. Matiašovský, Electrochim. Acta 37 (1991) 263.
[69] M. Makyta, G.M. Haarberg, J. Thonstad, V. Danek, J. Appl. Electrochem. 26 (1996) 319.
[70] D. Inman, S.H. White, J. Appl. Electrochem. 8 (1978) 375.
[71] A. Girginov, T.Z. Tzvetkoff, M. Bojinov, J. Appl. Electrochem. 25 (1995) 993.
[72] M. Makyta, P. Zatko, V. Danek, Influence of the melt structure on the deposition of molybdenum, titanium and aluminium, in: Proc. EUCHEM Conference on Molten Salts, August 1994, Bad Herrenalb, Germany, p. B-13.
[73] K. Matiašovský, V. Danek, M. Makyta, Koroze a Ochrana Materialu 20 (1978) 63.
[74] V. Danek, K. Matiašovský, Surf. Technol. 5 (1977) 65.
[75] V.G. Samsonov, V.A. Obolonchik, G.N. Kulichkina, Khim. Nauka Prom. 4 (1959) 804.
[76] C.J. Barton, L.O. Gilpatrick, J.A. Bornmann, H.H. Stone, T.N. McVay, H. Insley, J. Inorg. Nucl. Chem. 33 (1971) 337.
[77] V. Danek, I. Votava, M. Chrenková-Paucírová, K. Matiašovský, Chem. Zvesti 30 (1976) 841.
[78] J. Sangster, A.D. Pelton, J. Phys. Chem. Ref. Data 16 (1987) 506.
[79] O. Patarák, V. Danek, Chem. Pap. 46 (1992) 91.
[80] G.J. Janz, R.P.T. Tomkins, C.B. Allen, J. Phys. Chem. Ref. Data 8 (1979) 125.
[81] S. Cantor, D.P. McDermontt, L.O. Gilpatrick, J. Chem. Phys. 52 (1970) 4600.
[82] G.J. Janz, J. Phys. Chem. Ref. Data 17 (1989) 3.
[83] M. Chrenková, V. Danek, Chem. Pap. 45 (1991) 213.
[84] M. Chrenková, M. Hura, V. Danek, Chem. Pap. 45 (1991) 739.
[85] V. Danek, D.K. Nguyen, Chem. Pap. 49 (1995) 64.
[86] V. Danek, I. Votava, K. Matiašovský, Chem. Zvesti 30 (1976) 377.
[87] M. Chrenková, V. Danek, Chem. Pap. 44 (1990) 329.
[88] J.B. Bates, A.S. Quist, Spectrochim. Acta 31 (A) (1975) 1317.
[89] Z.A. Mateiko, G.A. Bukhalova, Zh. Neorg. Khim. 4 (1959) 1649.
[90] V. Danek, R. Cekovský, Chem. Pap. 46 (1992) 161.
[91] L.A. Harris, Acta Cryst. 12 (1959) 172.
[92] V. Bode, G. Teufer, Z. Anorg. Allg. Chem. 283 (1956) 18.

[93] G.D. Brunton et al., Report ORNL-3761, in: J. Braunstein, G. Mamantov, G.P. Smith (Eds.), Advances in Molten Salt Chemistry, vol. 3, Plenum Press, New York–London, 1975, pp. 336–358.
[94] Z.G. Goroshchenko, Khimia Titana, Naukova Dumka, Kiev, 1970.
[95] V. Danek, K. Matiašovský, Z. Anorg. Allg. Chem. 570 (1989) 184.
[96] V. Danek, J. Šiška, K. Matiašovský, Chem. Pap. 42 (1988) 753.
[97] K. Aotani, K. Hasegawa, Y. Miyazawa, J. Electrochem. Soc. Jpn. 27 (1959) 117.
[98] V. Danek, P. Fellner, K. Matiašovský, Z. Physik. Chem. Neue Folge 94 (1975) 1.
[99] R.V. Chernov, P.M. Ermolenko, Zh. Neorg. Khim. 18 (1973) 1372.
[100] D.K. Nguyen, V. Danek, Chem. Pap. 50 (1996) 4.
[101] V.A. Bloomfield, R.K. Devan, J. Phys. Chem. 75 (1971) 3113.
[102] W. Brockner, K. Torklep, H.A. Oye, Ber. Bunsenges. Phys. Chem. 83 (1979) 1.
[103] M. Chrenková, O. Patarák, V. Danek, Thermochim. Acta 273 (1996) 157.
[104] R.V. Chernov, P.M. Ermolenko, Zh. Neorg. Khim. 18 (1979) 2238.
[105] M. Chrenková, V. Danek, D.K. Nguyen, Z. Physik. Chemie 194 (1996) 51.
[106] D.P. Stuhl, H. Prophet, JANAF Thermochemical Tables, 2nd ed., NSRDS, Natl. Bur. Stand., Washington, 1971.
[107] A. Silný, V. Danek, D.K. Nguyen, Ber. Bunsenges. Phys. Chem. 99 (1995) 985.
[108] M. Chrenková, O. Patarák, V. Danek, Chem. Pap. 49 (1995) 167.
[109] M. Chrenková, V. Danek, A. Silný, Ber. Bunsenges. Phys. Chem. to be published.
[110] D.K. Nguyen, V. Danek, Chem. Pap. 51 (1997) 73.
[111] K. Grjotheim, C. Krohn, M. Malinovský, K. Matiašovský, J. Thonstad, Aluminium Electrolysis – Fundamentals of the Hall–Héroult Process, 2nd ed., Aluminium-Verlag, Dusseldorf, 1982.
[112] K. Grjotheim, B.J. Welch, Aluminium Smelter Technology, Aluminium-Verlag, Dusseldorf, 1988.
[113] K. Grjotheim, H. Kvande, Understanding the Hall–Héroult Process for Production of Aluminium, Aluminium-Verlag, Düsseldorf, 1986.
[114] W.E. Haupin, Light Metals 1995, Warrendale, PA:TMS, 1995, p. 195.
[115] B. Gilbert, G. Mamantov, G.M. Begun, Inorg. Nucl. Chem. Lett. 12 (1976) 415.
[116] B. Gilbert, T. Materne, Appl. Spectrosc. 44 (1990) 299.
[117] E. Robert, T. Materne, E. Tixhon, B. Gilbert, Vibrational Spectrosc. 6 (1993) 71.
[118] E. Grunert, Z. Elektrochem. 48 (1942) 393.
[119] J.F. Boner, Helv. Chim. Acta 33 (1950) 1137.
[120] M. Rolin, Ann. Phys. 6, Ser. 12 (1951) 970.
[121] G.A. Abramov, M.M. Vetyukov, I.P. Gupalo, A.A. Kostyukov, L.N. Lozhkin, in: The Theoretical Principles of the Electrometallurgy of Aluminium, Metallurgizdat, Moscow, 1953.
[122] T. Forland, H. Storegraven, S. Urnes, Z. Anorg. Allg. Chem. 279 (1955) 205.
[123] P.A. Foster, W.B. Frank, J. Electrochem. Soc. 107 (1960) 997.
[124] J. Brynestad, K. Grjotheim, F. Gronvold, J.L. Holm, S. Urnes, Disc. Faraday Soc. 32 (1961) 90.
[125] P.A. Foster, J. Am. Chem. Soc. 45 (1962) 145.
[126] M. Rolin, M. Bernard, Bull. Soc. Chim. France (1962) 423, 429, 939.
[127] A.I. Belyaev, E.A. Zhemchuzhina, L.A. Firsanova, Physikalische Chemie Geschmolzener Salze, VEB Deutscher Verlag für Grundstoffindustrie, Leipzig, 1964.
[128] K. Grjotheim, J.L. Holm, C. Krohn, K. Matiašovský, Svensk Kemisk Tidsskrift 78 (1966) 547.
[129] G. Petit, C. Bourlange, C.R. Acad. Sci. Paris 270 (1970) 937.
[130] J.L. Holm, Dr. techn. Thesis, The University of Trondheim, Norway, 1971.
[131] E.W. Dewing, Can. Met. Q. 13 (1974) 607.
[132] T. Førland, S.K. Ratkje, Acta Chem. Scand. 27 (1973) 1883.
[133] S.K. Ratkje, T. Forland, Light Metals 1976, Warrendale, PA:TMS, 1976, p. 223.
[134] B. Gilbert, E. Robert, E. Tixhon, J.E. Olsen, T. Østvold, Light Metals 1995, Warrendale, PA:TMS, 1995, p. 181.
[135] A. Sterten, Electrochim. Acta 25 (1980) 1673.
[136] S. Julsrud, Dr. techn. Thesis, The University of Trondheim, Norway, 1979.
[137] H. Kvande, Electrochim. Acta 25 (1980) 237.
[138] H. Kvande, Light Metals 1986, Warrendale, PA:TMS, 1986, p. 451.
[139] V. Danek, T. Østvold, Proc. IX Internet Symp. Light Metals Production, Tromso-Trondheim, Norway, August 1997, p. 9.
[140] J. Thonstad, A. Kisza, J. Kazmierczak, to be published.